Basin Research
August 2010, Volume 22, Issue 4, pages 398–413
http://dx.doi.org/10.1111/j.1365-2117.2009.00448.x

The definitive version is available at http://onlinelibrary.wiley.com/

Cenozoic mud volcano activity along the Indus Fan: offshore Pakistan

G. Calvès[1, *], A. M. Schwab[2], M. Huuse[1, 5], P. Van Rensbergen[3], P. D. Clift[1], A. R. Tabrez[4], A. Inam[4]

[1] School of Geosciences, Meston Building, Kings College, University of Aberdeen, Aberdeen, UK
[2] Marathon Oil U.K., Ltd, Marathon House, Rubislaw Hill, Aberdeen, UK
[3] Shell International Exploration and Production, Rijswijk, Netherlands
[4] National Institute for Oceanography, ST-47-Block 1, Clifton, Karachi, Pakistan
[5] Present address: Basin Studies Group, SEAES, The University of Manchester, UK.

*: Corresponding author : G. Calvès, email address : gerome.calves@laposte.net

Abstract:

This study documents the tectono-stratigraphic setting and expulsion history of a major, previously undescribed mud volcano (MV) province in the Indus Submarine Fan, offshore Pakistan. A buried MV field of nine composite MVs has been recognized using two-dimensional (2D) and 3D seismic reflection data in a confined area of 50 × 65 km^2. Conduits are recognized on each of these MVs connecting the pre-Eocene parent beds to the stacked mud cones. The buried MVs are up to 8.4 km wide (4.5 km average) with a central conduit of 1.23 km average diameter and an average mud cone thickness of 0.33 km. Three major phases of fluid and mud remobilization occurred in the Early to Middle Miocene, intra-Middle Miocene and in the Late Miocene to Plio-Pleistocene transition. Most of the mud source (parent beds) seems to be of pre-Eocene origin. Geometrical information from 21 mud cones allows an estimate of the volume required to build these fluid escape features. The calculated volume of remobilized sediments is 71.5±9 km^3. The location of the MV field is limited to the pre-Eocene main depocentre, with major tectonic deformation occurring along the wrench system of the Indo–Arabian plate boundary, i.e. the southern edge of the Murray Ridge. The Indus MV field is, to our knowledge, the longest lived (22 Myr) remobilized, Cenozoic sedimentary system observed worldwide. No evidence of present-day mud flow activity is seen on the seabed seismic reflection in the study area.

1. Introduction

Mud volcanoes (MVs) have long been a feature of interest in the Earth science community, with published observations dating back to 1866 (Anstead*,* reference in Kopf, 2002). Their occurrence onshore and offshore has been universally recognized in various geological settings from passive margins and accretionary prisms to fold belts (Milkov, 2000). Mud volcanism has been a research interest, in both academia and industry, where the focus has been on there relationship to green house effect, tectonic, fluid origin in relation to plate movement in accretionary prism, hydrocarbons and biology, but little in trying to understand the driving mechanism of the sediment remobilization process (Kopf, 2002).

Mud volcano edifices are recognized on seismic reflection data based on their geometries (single or stacked mud cones) and are often interbedded with background sedimentation (Newton *et al.*, 1980; Fowler *et al.*, 2000; Cooper, 2001; Evans *et al.*, 2007, 2008). The feeder system, or conduit, linking the parent bed to the mud cone is seismically inferred, or recognized, based on the transition from surrounding, well defined, parallel or sub-parallel reflections to chaotic reflections, associated in some cases with an increase in seismic noise. Modern 3D seismic and even 2D seismic technology can image mud volcano systems and their feeder systems in some detail, recently leading to the conclusion that “mud diapirs” interpreted on vintage seismic data are in reality stacked mud volcanoes and/or structural anticlines (van Rensbergen *et al.*, 1999). This distinction can be made when the size of the edifice is resolvable by the vertical and horizontal geometries, depending on the seismic resolution (van Rensbergen *et al.*, 1999; Graue, 2000; Stewart & Davies, 2006 and many other references).

The MV emplacement process is not presently completely understood. Two major geological processes may drive their initiation and location within basin marginal settings: high sedimentation rates in places such as the front of major deltas (e.g., Niger delta: Graue, 2000; Løseth, 2001; Baram delta: van Rensbergen *et al.*, 1999), and tectonic stresses, such as major shear or compression zones near plate boundaries (Brown, 1990; Henry *et al.*, 1990; Griboulard *et al.*, 1991; van Rensbergen *et al*., 1999; Kopf *et al.,* 2001; Chamot-Rooke *et al.,* 2005; Deville *et al.*, 2006). Implications for focused fluid expulsion of hydrocarbons (methane) have recently been reported from studies carried out in major petroleum provinces (Davies & Stewart, 2005; Cartwright, 2007). The rock physics (rheology) and fluid content/behavior of sediment layers could be the internal factors controlling the flow movement from particle-scale up to block-sized lithified rocks. Evolution of pore pressure and gas content are thought to be two major factors triggering the mobilization of the sediments from their mud source unit, which is often a regionally developed hydrocarbon source rock (e.g. Brown, 1990; Revil, 2002; Deville *et al.*, 2003; Maltman & Bolton, 2003). The Black Sea and Caspian Sea MVs could be seen as exception where the source of mud can be in some cases dissociated of the source rock (Yusifov & Rabinowitz, 2000; Graue, 2000). Examples of complex interaction between different stratigraphic source sediments, fluids and stresses (load, tectonic, temperature) (e.g. Dia *et al.*, 1999; Davies *et al.*, 2007) suggest that a single parent bed for the water-mud mix (Brown, 1990) cannot be a favored model in all mud-volcanism provinces.

The first observation of an offshore mud volcano (MV) in the Indus Fan southeast of the Murray Ridge was reported in 1990 (Fig. 1a) (Collier & White, 1990). Previously, mud volcanoes and mud 'diapirism' had been recognized in the on- and offshore region of the Makran, to the northwest of the Murray Ridge (Fig. 1a) (Stiffe, 1874; White & Louden, 1982; White, 1983). Recent seismic acquisition and onshore studies have been carried out in the Makran region with particular interest in the fluid dynamic and tectonic aspects (von Rad *et al.*, 1999*;* Delisle *et al.*, 2002; Ellouz-Zimmermann *et al.*, 2007). In the Makran region and the Arabian Sea, 24 onshore and more than four confirmed offshore mud volcanoes are reported in the compilation of Dimitrov (2000).

In this study we present a set of new data on the Indus Fan with observations on sediment remobilization (mud volcanoes) within the tectono-stratigraphic framework of the western Indian passive margin. We discuss the setting of the mud volcanism and the limitations on investigating some of the processes within the study area by using morphometric measurements, life span estimations and comparisons with other known mud volcano provinces worldwide.

2. Data set and methodology

Our seismic data set covers most of the western Indian passive margin from the Indus Delta to the Indus Fan, in the offshore Pakistan territorial area. The data used for the current study are 2D and 3D multi-channel, post-stack, time-migrated reflection seismic data (Fig. 1b). The seismic data displays in this study are zero phase, and have Society of Exploration Geophysicist normal polarity, i.e. black peak indicating an increase in acoustic impedance (Brown, 1996). Borehole information has been used to constrain the stratigraphy over this area (Calvès *et al.*, 2008) in conjunction with standard seismic stratigraphic principles (Vail *et al.*, 1977).

The 2D seismic data are 120-fold, with a 4 ms two-way time (TWT) sample rate. There are two vintages of acquisition: 1977 (reprocessed in 1999) and 1999. The total survey length is about 2042 km. The frequency content ranges from 5 to 70 Hz. The 2D grid spacing ranges from 2.5 to 8 km (Deptuck *et al.*, 2003). The 3D seismic survey covers an area of 725 km^2 (two blocks, labeled 3D-T1 and 3D-T2 in Fig. 1b) and is 120-fold with a 4 ms TWT sample rate. The 3D grid is subdivided into inline and cross-line directions, spaced at 25 m and 12.5 m respectively. The frequency range in the shallow subsurface is 7.5–90 Hz, with a dominant frequency in the 25–50 Hz range.

Depth conversion of time structure maps is based on a layered velocity profile constrained by seismic stacking velocities. The water velocity is assumed to be 1.5 km/s, and the bulk sedimentary section has a mean interval velocity of 3.3 km/s. The pre-Eocene sequence has a 3.0–3.5 km/s interval velocity (discussed below). A detailed analysis of the local velocity profile was done to determine the size dimensions of the individual mud cones and conduits. It is important to note that we have not applied any decompaction factor to the sediments. This deliberate choice was made in order to keep the described examples at an observational level. Application of a decompaction component would add another uncertainty to the ones already implied by interpretation, time-depth conversion, uncertainties in the actual physical sediment properties, and lack of knowledge of how the mud volcano has compacted.

The study area is not covered by multi-beam bathymetry or side-scan sonar data. No seabed or subsurface samples of the mud volcano field have so far been recovered.

3. Observations

The mud volcano field observed in the subsurface and partially at the seafloor is developed on the continental slope of the western Indian passive margin in water depths between 400 to 1400 m in front of the Indus Delta (Fig. 1b). Nine mud volcanoes composed of a total of twenty-one individual stacked mud cones are mapped based on their maximum extension observed on both the 2D and 3D reflection seismic data. The names of the mud volcanoes are inherited from a study conducted by Shell Exploration and Production (E&P).

3.1 Tectono-stratigraphy

The slope of the observed margin is confined to the northwest by the plate-boundary between India and Arabia (MR: Murray Ridge), which divides the northeast Arabian Sea into two major morphological areas, the Indus Fan and the Makran Accretionary Prism/Gulf of Oman (Fig. 1a). The study area thus consists of two contrasting tectonic regimes. To the northeast the area is bounded by extensional growth faults on the continental shelf (NW-SE trend) and to the northwest by strike-slip faults that define the plate boundary along the western edge of the Murray Ridge (Fig. 2) (Calvès *et al.*, 2008). The stratigraphic record covers the Cenozoic, with Paleogene infill of the margin post-dating the last rifting event associated with the Deccan volcanic-igneous event ~65 Ma (Calvès, 2009). This sequence is followed, at about 24 Ma, with the initiation of the Indus Fan (Clift *et al.*, 2001).

Three major phases of tectonic activity are recorded in the Indus Fan and its underlying basement. Initial shear events, tentatively dated as post-Cretaceous, are recorded by pull-apart type geometries with a NE-SW sense of extension (Figs 2a, 2b and 3a) (Calvès *et al.*, 2008). This is followed by a more tectonically stable phase of sedimentation during the pre-Eocene period. At the Eo-Oligocene transition, the basin experienced further strike-slip deformation, resulting in inversion of the infilled pull-apart sub-basins and the growth of folds along N-S axes. During the Early Miocene, the strike-slip faulting was reactivated and over-printed the major folds near the edge of the Indus Fan along the Murray Ridge (Calvès *et al.*, 2008).

The basement depth ranges from ~5 km in the west (Murray Ridge) to >9.5 km in the south of the study area (Fig. 3a). A major trough is developed along a NNE-SSW trend. The basement is affected by strike-slip faults with a NNE-SSW principal component (parallel to Murray Ridge) in the west, whilst normal faulting is present in the east along a lineation oriented NNW-SSE, parallel to the present day continental shelf (Fig. 3a). The base of the stratigraphic interval of interest is calibrated on a regional seismic event equivalent to the top of the syn-rift volcanic sequence that is associated with the transition from the Upper Cretaceous to the base of Paleogene (Calvès, 2009). The lower sedimentary sequence referred to in this paper could be dated from the base of the Paleogene to the base of the Eocene. For simplicity, we will refer to this sequence as pre-Eocene. The depth to the top of the pre-Eocene ranges from <5 to ~8.25 km (Fig. 3b). Anticlinal structures are observed on seismic sections (Fig. 2) with N-S or NW-SE axes, plunging to the south or southeast respectively (Fig. 3b – dashed black lines). Mud volcanoes are mainly located on top of high structures/anticlines at the top of the pre-Eocene. The isopach between the basement and top pre-Eocene stratigraphic horizons shows the location of the main pre-Eocene depocenter (Fig. 3c). Thickness of this interval ranges from <0.5 km to >1.5 km. The core of the sediment is deposited along two bodies that trend NE-SW and are over 1 km thick. In Fig. 3d, the isopach map of Neogene sediment from top pre-Eocene to the sea bed shows an overall gradual east to west thinning towards the Murray Ridge, with local variations in the vicinity of the folds.

Mud volcanoes are observed in association with the pre-Eocene depocenter, and areas of basement-involved, as well as detached deformation of the top pre-Eocene along an E-W direction (Fig. 2) near the inverted pre-Eocene depocenter (sub-basins) (Fig. 3c). MVs are generally well preserved (in stratigraphic intervals) with onlap surfaces on their flanks.

3.2 Mud volcano field description

Because of the excellent seismic imaging of the MVs, the present day mud volcano field can be qualitatively and quantitatively assessed. Morphometric description is based on the parameters illustrated in Fig. 4. The following characteristics are measured from 2D or 3D seismic data when recognized: mud cone diameter (Dmc), height (thickest part of the mud cone - Hmc), conduit height (base is measured from the top of the parent bed and the top is the base of the mud cone – Hc and Dc), and crater width. Other measured parameters at the vicinity of each mud volcano and for sequential mud cones are: parent bed thickness (Pbt), basement depth (Bd), overburden thickness at the mud volcano base (Omb) and depth to the top of the pre-Eocene (Pd) (Fig. 4). Each conduit is characterized seismically by the transition from coherent to chaotic reflection packages from the outer to the inner part of the mud volcano edifice and a vertical connection from the parent bed to the mud cone (c.f. following section and Fig. 5). A volumetric estimation of mud cones is based on the assumption of a conical geometry and the conduit as a simple cone instead of a cylinder (Fig. 4).

3.3 Seismic reflection image description

3.3.1 Depositional versus remobilized features

Some generalized 2D seismic examples from the study area illustrate the seismic characteristics used to distinguish deep-water sedimentary bodies, such as channel-levee systems, from sediment mobilization features, such as mud volcanoes (Fig. 5). Three seismic examples, from shallow to deeper subsurface, show how we observe and interpret these features in relation to different depths. In Fig. 5a, which is representative of images in the shallow subsurface (0–1 s TWT below seafloor), continuous reflections are observed in which some terminate in classic patterns of onlap, downlap, toplap or erosional truncations. Three main types of seismic geometries and facies can be observed: 1) intervals of parallel, continuous reflections, 2) areas of wedge-shaped continuous reflections of variable amplitude that are sub-parallel, and 3) areas of stacked, wedge-shaped transparent seismic facies with high amplitude reflections at the edge. These main types of seismic facies can be interpreted as resulting from: 1) background slope, deep-water sedimentation, 2) channel-levee complexes, 3) mud volcanoes made of stacked mud cones, respectively.

The mud volcanoes show a characteristic, Christmas tree geometry derived from stacking mud cones (Yielding & Travis, 1997; Somoza *et al.*, 2002; Stewart & Davies, 2006) and are characterized by a well-defined outer ring and an inner domed cone (Fig. 5a). The edifice is made of successive gas-enriched mud flows or mud breccias, which are observed as transparent seismic facies. In Fig. 5a, the width to height ratio is one to three for the mud volcano and four to one for the channel-levee complex. Figure 5b shows the geometry of a channel-levee complex buried 1.5 to 2 s TWT below the seafloor. On this seismic line concordant, parallel, continuous reflections can be traced across the entire seismic profile. The base of the channel-levee complex can be inferred from the erosional truncation at the base of the channel and the downlap termination at the base of the levee transparent seismic facies. The top of the channel is faint but can be delineated by the onlap surface at the edge of the levee. Figure 5c represents an image of a deeper part of the section (2 to over 3 s TWT below the seafloor) and illustrates the contrast between a channel-levee complex and a mud volcano on seismic images. Again seismic reflection terminations and seismic facies allow the recognition of a channel-levee complex and mud cone-conduit system within a concordant, continuous stratigraphic section. In this example the scale comparison between channel-levee complex and mud volcano is different from that shown in Fig. 5a. In width the levees are more extensive than the mud volcano, whilst the thickness of the mud cone is two-times greater than the associated levee. The geometry of a channel-levee system along a shelf-basin profile evolves with changing slope and processes, as discussed previously (Kolla & Coumes, 1987; McHargue & Webb, 1986; Deptuck *et al.*, 2003), while the geometry of a mud volcano is more localized, comprising vertically stacked mud cones.

One very distinctive difference between a mud volcano and a channel-levee geometry is the recurrent presence of highly disturbed reflections below and in the core of the mud cone. This can only be seen if the seismic lines cross the conduit of the mud volcano, otherwise the interpretation must rely on the reflection geometry and seismic facies analysis.

3.3.2 Detailed geometry and stacking of mud volcanoes

Seismic images of mud volcanoes displayed in vertical seismic sections (Figs 6a and b) and two horizon time structure maps associated with a coherency extraction (Figs 6c and d) illustrate the different observations developed in this section. Geometric and stratigraphic measurements of all studied mud volcanoes are summarized in Table 1.

Three of the nine mud volcanoes occur in the 3D-T2 seismic survey (MVs *Louise*, *Joyce* and *Georgina*, Fig. 1). The shallowest expression of sediment remobilization is illustrated by MV *Louise* (Fig. 6a). This MV shows a classic Christmas tree geometry with mud flows interdigited with the background sub-parallel seismic reflections and dome shaped mud cones. The core of the composite dome contains chaotic to transparent seismic reflections. A series of four potentially different mud cones are highlighted (Fig. 6a). Two more deeply buried MVs (MV *Joyce* and MV *Georgina*) occur to the SSW, and to the NW of MV *Louise*. These are stratigraphically overlain by channel-levee complexes expressed by high-amplitude reflection packages – channel type and transparent low reflectivity seismic facies-levee type (Fig. 6b) (e.g. Deptuck *et al*., 2003 and references within). The mud cones (MV *Joyce* and MV *Georgina*), between the yellow and blue stratigraphic horizons (colored arrows in Fig. 6b), have a wedge geometry and are marked at the top and base by bright negative amplitude reflections. Observations in 3D allow their differentiation from a classic channel-levee complex. They are associated with two main features, the first is the presence of chaotic, disturbed reflections separating the wedge-wing geometry (conduit), and secondly by the geometry of the surrounding strata, convex downward at the base and convex up at their top (Fig. 6b). These two last observations are related to the emplacement process of mud volcanoes, anticlinal-faulting and sinking of the mud crater after activity, and differential compaction or remobilization of sediment at other stages of growth. Figures 6c and 6d show the stratigraphic arrangement of the three MVs. The blue horizon time structure map (Fig. 6c) shows a slope from NE to SW with disturbed areas related to the *Louise* MV, which is easily identified on the time structure map between the 1.65 and 1.7 s TWT contours. An amplitude map displays a mud flow can be seen running off the south side of the mud crater and extending out about 5 km along the slope (Fig. 6c, white and black dotted lines).

MV *Georgina*, lying on the isotime contour 3.1 s TWT, displays a trough shape potentially related to subsidence above the conduit (collapse/compaction) (Fig. 6d). MV *Joyce* corresponds to a structural high surrounded by the isotime 3.35 s TWT contour. This volcano geometry allows delineation of the outer ring of the mud cone. Coherency extraction at this stratigraphic horizon, allows features such as calderas, craters, conduits, and faults to be defined (Fig. 6d). At the yellow horizon stratigraphic level the following summary of activity can be made: MV *Joyce* was active, MV *Georgina* was at the sinking stage, and MV *Louise* had not yet developed although the conduits later pierce this surface (Fig. 6d).

MV *Louise* shows the latest stage of sediment remobilization, which occurred during and after channel-levee complex deposition, resulting in an anticlinal structure at shallow levels (Figs 2b and 6a). The upper surface that we present corresponds to an amplitude map along the blue stratigraphic horizon (blue arrow). A mud flow escaping from MV *Louise* is observed, followed by later stages of mud cone development in a parallel-bedded, draping sedimentary system (Figs 6a and c). On top of MV *Georgina* faults that initiated at the apex of the last cone offset the subsequent sedimentary sequences. These could be potentially related to a later relaxation stage of the system at this location (Figs 6b and c).

No mud sills are observed or identified in the study area. We make a deliberate choice of not using mud diapirism to explain the geometries observed because specific anticlinal structures are clearly imaged on this high quality seismic data.

3.4 Pressure conditions at the present

Overburden pressure, lithostatic pressure, and vertical stress are terms that denote the pressure or stress imposed on a layer of sediment by the weight of overlying material (Osborne & Swarbrick, 1997). Using the velocity information from the processing of seismic reflection data and the geologic framework, we have extracted a velocity-depth profile to help detect any intervals of significant overpressure in the mud volcano substrate (Fig. 7a). A normal velocity increase with depth is observed up to 4–5 km below the sea floor, suggesting that sediments above these depths are normally compacted with hydrostatic pore pressure. Below that depth, a velocity decrease is observed at some locations. This could be related to a change in either lithology, or porosity, or both, and could indicate overpressure (Osborne & Swarbrick, 1997; Bell, 2004). The depth of the anomalously low velocities largely coincides with the pre-Eocene interval inferred to be the likely mud volcano parent unit based on seismic stratigraphic evidence. We further investigated the cause of the velocity anomaly using a simple model-based approach to estimate the potential present-day pressure in the Indus Fan subsurface (Gutierrez & Wangen, 2005).

Pressure-depth plot computations are based on the following parameters: sea water density 1024 kg/m^3, formation water density 1070 kg/m^3, and a porosity-depth curve from Sclater & Christie (1980), which is calibrated and consistent with regional porosity-density-depth information (Bachman & Hamilton, 1976; Velde, 1996; Clift *et al.,* 2002). The average density of sediment particles/grains is assumed to be a constant value of 2750 kg/m^3 (Bachman & Hamilton, 1976). A normal gradient of 0.23 MPa/m (1 psi/ft; black continuous line) for lithostatic pressure and a hydrostatic gradient of 0.01 MPa (0.45 psi/ft; dashed black line) are plotted for reference (Converse *et al.,* 2000) (Fig. 7b). Lithostatic curves are plotted for both 668 and 1315 m water depth. An additional set of lithostatic pressure curves is plotted for varying porosity-depth relationships (grey continuous lines) to illustrate the potential differences between linear and non-linear lithostatic pressures (i.e. porosity effect) (Fig. 7b).

At the depth of the pre-Eocene parent bed in the vicinity of the MVs (5.6–8.5 km sub-seafloor) we would expect, based on the model illustrated in Fig. 7, hydrostatic and lithostatic pressures ranging between 55–75 MPa and ~110–205 MPa, respectively. We have plotted a tentative pore pressure profile (gray dashed line) and the fracture gradient, which is assumed to be 75% of the lithostatic pressure at any given depth (Fig. 7b). Maximum overpressure, defined as the difference between the hydrostatic and the fracture gradient at the minimum depth of the pre-Eocene, is approximately 30 MPa (~4.3 kpsi). Qualitatively, it would seem that the parent unit is still under significant overpressure (under-compaction), although not enough to drive an active mud eruption.

4. Discussion

4.1 Timing – sedimentation rates – tectonic stress

Relative one-dimensional average sedimentation rates were calculated in the vicinity of each mud volcano in an area where the stratigraphy is not too disturbed by major dipping structures (i.e. anticlines, stratigraphic pinch-outs, erosional truncations) or unconformities, or by the mud cones themselves.

It is important to note that no stratigraphic hiatus was used to constrain the 'real' sedimentation rates in the area because of a lack of detailed biostratigraphic information in the section. This could lead to potentially underestimating the sedimentation rates during a given window of time in the sedimentary record. Therefore the following sedimentation rates are considered relative.

Average sedimentation rates for the defined stratigraphic intervals are: pre-Eocene 95 m/myr, Eo-Oligocene 68 m/myr, Lower Miocene 189 m/myr, Middle Miocene 342 m/myr, Upper Miocene 106 m/myr, Pliocene 32 m/myr, Pleistocene 85 m/myr (Fig. 8). Equivalent variation trends through the Cenozoic have been described previously by different authors with relationships between fluxes of sediment, tectonic and atmospheric processes proposed in the region (e.g. Métivier *et al.,* 1999; Clift, 2006). Rapid sedimentation on the margins around South and Southeast Asia during Early and Middle Miocene time correlates with the development of major deltas and increased erosion in the source areas. This would correspond to the enhanced development of the Indus Fan in the study area.

As shown in Fig. 8, major phases of mud volcanism seem to occur either during tectonic events and/or during periods of high sedimentation rates. It is known that the occurrence of mud volcanoes on passive margins is well correlated with several factors, such as (1) thick, rapidly deposited sediments, (2) Tertiary age, (3) tectonic stress, especially shortening, (4) sediment overpressuring and fluid migration, and (5) density inversion (summarized by e.g. Milkov, 2000; Kopf, 2002; Judd & Hovland, 2007).

4.2 Geometric observation – paleo activity

Certain aspects of mud cones can be associated with types of activity because the edifice geometry is controlled by the viscosity and consolidation of the extruded material (Henry *et al.,* 1996; Ivanov *et al.,* 1996; Kopf, 2002; Yusifov & Rabinowitz, 2004). Some of the early observations in the Gulf of Oman and at the northern edge of the Murray Ridge (Fig. 1a) (White, 1983; Collier and White, 1990) may be debatable in terms of data quality and interpretation. For example, it is important to note that the mud volcano at location 4 in Collier and White (1990) (equivalent to the present study area) is not shown in their paper. The ‘shale diapir’ and mud volcanoes interpreted at that time were based on a “*‘pear’ shaped and acoustically transparent region”,* which are in fact buried deep-sea channel-levee complexes (Fig. 5) (c.f. Gaedicke *et al.*, 2002; Ellouz-Zimmermann *et al.*, 2007).

Using the dimensions of observed mud cones, we have plotted the height-width data of each mud cone to investigate the range of overall cone slope (Fig. 9). Again these values are considered without decompaction of the cones. A linear dotted line of about 5º slope is plotted for reference to show variation around this value for the mud cones observed. The heights of cones range from 85 m to 640 m, while observed widths range from 800 m to 8440 m. Specific data points deviate from the 5º slope, but remain within the 2–11º range .The first mud cone at each MV location is plotted with a black dot (Fig. 9). No specific correlation between timing and slope seems to occur from our mud cone aspect investigation. Nevertheless, the range of values are in the order of those observed in shallow buried or active MVs in most known offshore mud volcano fields, such as El Arraiche (Gulf of Cadiz), Barbados and the South Caspian (Henry *et al.*, 1990; Yusifov & Rabinowitz, 2004; van Rensbergen *et al.*, 2005).

The depth relationship between mud cone base and parent beds, i.e. Hd, is investigated in Fig. 10. This shows no correlation except for showing the overburden thickness necessary to initiate mud volcanism at the surface. For deep seated mud cones, and considering compaction for the older events (mud cones), a minimum value of over 1.5 km overburden thickness would be necessary to develop sufficient stress for the parent bed to become overpressured and trigger escape. The youngest MVs in the area show overburden thicknesses of 3.2–7.4 km (MV *Louise* and MV *Anne* respectively in Fig. 10). This range of minimum parent bed overburden has also been observed in the offshore Niger Delta, where minimum values of 1–2 km overburden were recorded overlying the source layers at the time of mud volcanism initiation (Graue, 2000). In the South Caspian Basin values are over 2 km of overburden for the *Chirag* MV (Davies & Stewart, 2005).

4.3 Volumetric considerations

The study area covers an area of ~3250 km^2 (Fig. 1). A bulk undercompacted sediment volume of ~21,755 km^3 is estimated between seafloor and the volcanic basement of Cretaceous age, based on depth converted surfaces in this area (Figs 1 and 2 a). The isopach map extracted for the pre-Eocene interval estimates a volume of 2625 km^3, corresponding to 12% of the gross Cenozoic volume. Results of a simple cone volumetric estimate for each mud cone and volcano in the study area (Table 1) represent a total volume of 71.5 ± 9 km^3 of sediment remobilized, which is equivalent to 2.7% of the presumed main parent pre-Eocene source unit and ~0.3% of the Cenozoic bulk sediment volume. Assuming a continuous connection between the source beds and the mud cones by a conduit of conical geometry, we can estimate a second volume of remobilized sediment. The bulk volume associated with these conduits is estimated to be 17.6 ± 3.5 km^3.

This estimate does not take into account the volume of mud expelled beyond the edge of the mud cones. This volume could be as large as that observed in the mud cone themselves if we assume that the productivity of the mud volcanoes was sufficient to expel mud from the ring of the cones at the paleo-seafloor. Note that all volumes are in their present, compacted state.

The volumetric results presented here (MV *Ingrid* ~20.5 km^3) are of the same order as buried mud volcanoes present in the South Caspian, e.g. *Chirag* MV ~22.5 km^3 (Stewart & Davies, 2006).

4.4 Long term fluid expulsion

Mud volcanoes are acknowledged to contribute to the transfer of gases from the solid Earth system to the atmosphere and the oceans depending on where they occur (on- or offshore) (Milkov, 2000, 2003; Dimitrov, 2002; Kopf, 2002, 2003; Judd *et al.,* 2002). In the present study we have estimated mud volcano volumes in the Indus Fan throughout the Cenozoic. Because of the uncertainties implied throughout the different stages of our study and the small estimates of long-term gas emission, we use a conservative volumetric computation for fluid flux, as suggested by Kopf (2003). The long duration of this mud volcano field throughout the Cenozoic leads to uncertainty because previous estimates of fluid flux have been made on much shorter time spans. Other potentially important fluid volumes (e.g. water, CO_2, CH_4, hydrocarbons) released to the ocean and potentially reaching the atmosphere can be estimated from the volume of remobilized sediment (e.g. Sauter *et al.*, 2006; Naudts *et al.*, 2006; Leifer *et al.*, 2006; Greinert *et al.*, 2006). Following previous estimates of average fluid flux associated with large offshore mud features (> 1 km in diameter), we postulate a value of 10^6 m^3/y for the average fluid flux from the mud volcano field in the study area (Kopf, 2003). We conclude that mud cones are built over similar time periods as channel-levee complexes or deep sedimentary features, i.e. 3rd to 4th order in a classic sequence stratigraphic analysis, 10^5–10^6 years (e.g. *Clift et al.,* 2002; Hadler-Jacobsen, 2007). To obtain a conservative estimate of the time necessary to build a mud cone, we compute a life span estimate calibrated on mud cone height and average sedimentation rates over the stratigraphic interval of their occurrence. This analysis results in values of 2.0–2.5 Myr on average for the 20 mud cones observed with a minimum of 0.6 Myr (shallow cones MV *Louise*) and a maximum of 5.6 Myr duration (first observed deep cone at MV *Ingrid*). The average total life span of MVs over 2 or 3 Myr is related to the long duration of the Early Miocene (>7.4 Myr) for which we have biostratigraphic control. In reality the volume of fluids associated with the sediment remobilization could have been expelled at multiple times during the history of the basin.

The cyclicity of long-term mud volcano field development in sedimentary basins is poorly constrained and understood. Mud volcanism provinces (buried or shallow) of interest to the oil industry have good constraints on relative age and timing of mud extrusion.

Assessment of the time constraints on mud volcanism in the South Caspian suggest that it has been active since 4.33 Ma (Yusifov & Rabinowitz, 2000). Similarly, the offshore Niger Delta shows evidence for mud volcanism since 2 Ma (Graue, 2000). Another example, the Shah Deniz mud volcanoes in South Caspian Sea (Fowler *et al.*, 2000), interestingly shows delayed development between structuration of the basin and the occurrence of mud volcanism on the order of 0.5 to 1 Myr. In the Mediterranean Ridge accretionary complex, estimates from seismic reflection data, scientific boreholes and biostratigraphy, show episodic eruptive activity over periods of ~1 Myr, with as little as ~0.3 Myr on one particular mud volcano (Kopf & Behrmann, 2000; Robertson & Kopf, 1998).

Based on these estimates (volume of sediment remobilized and average flux for offshore large and mid-sized mud volcanoes (Kopf, 2003)), the emission of fluids (e.g. gas) associated with mud remobilization in the area since the start of the Neogene could have been equivalent to a bulk volume of 4.93×10^4 km^3 ($\pm 10^1$ km^3). It is important to note that no major bottom-simulating reflector (BSR) related to hydrate saturation in the sediments is observed at the top of the shallowest observed MV, with the exception of the more distal MV, which is located towards the Murray Ridge (MV *Anne*), the plumbing system of which was described in Calvès *et al.* (2008). It seems clear that this margin has been under extensive fluid expulsion, as recorded by these massive sediment remobilization edifices, but that at the present day no major flow of fluids has yet been observed.

The potential correspondence between mud volcanism and hydrocarbon generation in the area is not proven, but by comparison with other similar provinces such as the South Caspian, Niger Delta (i.e. pulses of high sedimentation rates, structuration of the basin, compression on potential parent beds at high pressure in depth (Hedberg, 1980)) the paleo-production of hydrocarbons associated with mud volcanism could be considered as a plausible driver of mud mobilization and extrusion in the Indus Fan.

4.5 Model for mud volcanism

The occurrence of mud volcanism in the Indus Fan is synthesized in a diagram showing the evolution of the margin in six main steps, with a focus on the tectonic and stratigraphic framework (Fig. 11). Following the end of rifting along the western Indian margin ~65 Ma and a major phase of volcaniclastic deposition related to the Deccan event (Fig. 11a), the margin in the study area comprised a set of normal faulted blocks and pull-apart geometries (potential shear in the crust). During the pre-Eocene, these sub-basins were infilled by sediment, while carbonate platforms developed on the highest topographic structures along the margin (Fig. 11b). Close to the transition from the Paleogene to the Neogene (~24–21 Ma (Clift *et al.*, 2001)) a major shearing tectonic event affected the basin by uplifting the Murray Ridge and inverting the sub-basin pre-Eocene infill into anticlinal structures (Fig. 11c). This event is marked by initiation of the first mud volcanism activity at MV *Ingrid* and MV *Joyce* with parent beds of pre-Eocene source (Figs 8 and 11c). During the Neogene the margin changes character to a prominent delta-slope-deep water sedimentary setting (Fig. 11d). This is marked by high sedimentation rates and loading over the anticlinal structures present in the distal portion of the study area. This load accentuated the structures by adding vertical stress under the delta wedge and a compressive East-West component. During most of the Miocene the study area was comprised of a combination of sedimentation types: prograding deltas (continental shelf), canyon incision (Figs 11d and e) (Kolla & Coumes, 1987; Droz & Bellaiche, 1991; Deptuck *et* *al.,* 2003), and channel-levee complex development in the slope and deep basin. Most of MVs show activity during that period (Fig. 8). During erosion of the slope by canyons and channelization, mud cones were not preserved. It is important to consider that this local 'unloading' could have terminated the build-up of overpressure in the parent beds. During the latest Early Miocene and early Middle Miocene another shear stress is added over the present structures (Figs 8 and 11e) (Calvès *et al.,* 2008) and the continental shelf changes to a growth fault setting, with the pre-Eocene interval acting as a décollement surface. During the Plio-Pleistocene, the margin experienced the last mud volcanism event (MVs *Louise*, *Catherine* and *Anne*) with an overall decrease in sedimentation rates. The mud volcanism appears to have ceased around the Pleistocene, with draping of the mud cones (Fig. 8). The present day the basin does not exhibit mud volcanism activity (Fig. 11f).

Seismicity could be a triggering mechanism for sediment remobilization of fluid flows in the study area. Despite the location on the active plate boundary of the Murray Ridge seismicity is limited compared to that seen onshore (http://earthquake.usgs.gov/regional/world/seismicity/m_east.php; Sykes & Landisman, 1964). This is different from the nearby Makran province where following the earthquake of 1945, the birth of an island associated with mud volcanism was documented (Sondhi, 1947 reference in Delisle, 2004).

4.6 Comparison of the Indus Fan mud volcano field with other off-shore provinces

The height vs. surface area of mud cones in the Indus Fan has been plotted along with a compilation of such data from published studies. Our compilation places the Indus Fan MVs among the largest and in particular thickest MVs recorded, only exceeded by the giant *Chirag* MV in the Caspian (Fig. 12). This is despite our lack of correction for compaction.

Of note is that this data is based on only nine mud volcanoes recognized in the area due to the sparse 2D seismic data coverage. This province could be one of the longest active (~22 Myr in multiple phases) MV provinces recorded in a Tertiary basin worldwide.

5. Conclusion

Based on seismic reflection data, nine mud volcanoes composed of twenty-one (individual) mud cones were defined and placed in a tectono-stratigraphic framework.

In the present study we document an extensive and prolific mud volcano field that occurred from the late Paleogene to nearly the Plio-Pleistocene, making the Indus offshore mud volcano field the longest lived province ~22 Myr known worldwide. Initiation of mud volcanism is related to two aspects: 1) high sedimentation rates over short geological periods (initiated here at the base of the Neogene with accelerated sedimentation on the Indus Fan off the western Indian margin), and 2) tectonic stress, as in other equivalent geological settings where mud volcanoes are recognized (e.g. in front of a major delta and/or near plate boundaries). We described the morphometric characteristics of the mud volcano field in relation to the limitations of the seismic data set. The measured elements make this mud volcano province one of the most impressive, with mud cones up to 8.4 km wide, thicknesses up to 0.64 km, and volumes of up to 23.5 km^3 of remobilized sediments. The minimum overburden thickness at which mud is remobilized from deep sources in the basin (pre-Eocene parent bed) seems to be on the order of 1.5 to 2.0 km. Further investigation and modeling of this system could lead to an understanding of the long-term evolution of such large-scale sediment remobilization activity within this sedimentary basin. This, in conjunction with the maturity of *in-situ* organic matter within the sedimentary pile, could contribute significantly to the driving forces behind sediment remobilization from deep in the basin up to the (paleo-) seafloor.

Acknowledgments

We would like to thanks NIO-Pakistan and Shell for access to the data set and for allowing publication of this work. GC's PhD scholarship was funded by the University of Aberdeen. Thanks to SMT-Kingdom® and Landmark® support for university software grants. The present study reflects only the authors view. We thank also R. Davies, E. Deville and an anonymous reviewer for providing helpful comments and suggestions.

Figure and Table captions

Figure 1: Location map of the study area (a), recognized mud volcanoes or mud 'diapirism' features in the Arabian Sea and Makran Accretionary Prism are plotted as stars (White, 1983; Collier *et al*., 1990), circles (e.g. Delisle *et al*., 2002) and triangles (Ellouz-Zimmermann *et al.*, 2007 and references within). Sea bed depth map, the study area is located in 400 to 1400 m water depth, contour interval 100 m (white lines). (b) Location of mud volcanoes are plotted in thick black circles. Black lines are 2D seismic and 3D seismic

surveys are in white dashed boxes. A-A' and B-B' seismic profiles along depositional dip shown in Fig. 2a and Fig. 2b.

Figure 2: Regional E-W line drawings showing basin tectono-stratigraphy with the location of mud volcanism (black mud cones). Location of seismic profiles is plotted on Fig. 1b.

Figure 3: (a) Basement depth structure map with major faults annotated. (b) Top pre-Eocene depth structure map. (c) pre-Eocene sediment isopach map. (d) Top pre-Eocene to seabed sediment isopach map. Dark colours are deeper or thicker areas. Mud volcano locations are noted as black circles for reference and anticline axes or thick depocenters are black dashed lines.

Figure 4: Schematic diagram of dimensions measured for mud volcanoes in this study. Dmc: diameter of mud cone, Hmc: maximum thickness of mud cone, Hc: Height of conduit from parent bed top to base of mud cone, Dc: maximum diameter of conduit, Pd: parent bed depth below seafloor, Omb: overburden over parent bed at base of mud cone, Bd: basement depth below seafloor, Pbt: parent bed thickness.

Figure 5: Illustrated seismic lines and observations used to differentiate MVs from channel-levees. (a) shallow subsurface example, (b) deeply buried channel levee, and (c) deeply buried MV and channel-levee.

Figure 6: (a, b) Seismic examples of MVs at different burial depths. Note the vertical scale of A is twice that of B to show reflection detail. Note two stratigraphic horizons (blue, yellow). (c, d) Coherency extraction along a stratigraphic horizon blended with a time structure map of the horizon in colour illustrating the mud cones, mud flows, conduit locations and faults that develop around them. C is the blue horizon and D is the yellow horizon. Note that C also shows an amplitude and coherency map of the blue horizon.

Figure 7: (a) Sea water to base overburden interval velocity–depth plot illustrating the normal compaction trend, minimum and maximum depth of pre-Eocene sequence which contains the MVs with velocity drop related to potential lithology change and/or overpressure in this interval. (b) Diagram illustrating pressure-depth profiles from physical data in the area projected to depth of the pre-Eocene sequence around the MV locations. Water depth range: 668 – 1315 m.

Figure 8: Tectono-stratigraphic summary of mud volcano occurences during the Cenozoic in the Indus Fan record. Relative sedimentation rates are plotted according to the stratigraphic framework and depth converted intervals in the vicinity of the mud volcanoes. Sedimentary features: channel-levee complex (C.L.C.), erosional truncation (E.T.), draping (D.), mud cone (M.C.), tectonic regime (T.), growth faulting (G.F.), inversion (Inv.) and shear (S.).

Figure 9: Mud cone aspect diagram as a function of height and width in kilometers. Dotted line represents a slope of about 5°. The first buried mud

cone at a given location is represented by a black dot and subsequent younger cones by white dots.

Figure 10: Diagram of overburden thickness at the bases of mud cones (post – pre-Eocene) plotted against parent bed interval thickness (pre-Eocene). First buried mud cone at each location observed is represented by a black dot and subsequent (younger) cones by white dots.

Figure 11: Schematic block diagrams of the Cenozoic tectono-stratigraphic evolution of the margin highlighting the occurrence of associated mud volcanism. CLC – channel-levee complex. MV – mud volcano. BSR – Bottom Simulating Reflector.

Figure 12: Position of the Indus Fan mud volcano field as height-surface of cones compared to other MV provinces (white filled triangles, Barbados: Henry *et al.*, 1990; grey filled triangle, South Caspian giant MV: Davies & Stewart, 2005; black cross, El Arraiche: van Rensbergen *et al.*, 2005; grey diamonds, South Caspian: Evans *et al.*, 2007; white filled dots, South Caspian: Yusifov & Rabinowitz, 2004; grey dots, Indus Fan: this study). The plot places the Indus MV cones among the thickest and largest of the published examples considered.

Table 1: Geometric data of MVs extracted from seismic data in the study area (see Fig. 4 for explanation).

References

BACHMAN, R.T. & HAMILTON, E.L. (1976) Density, porosity, and grain density of samples from Deep Sea Drilling Project Site 222 (Leg 23) in the Arabian Sea. *J. Sediment. Res.*, **46**, 654–658.

BELL, D.W. (2004) Velocity estimation for pore-pressure prediction. In: *Pressure regimes in sedimentary basins and their prediction* (Ed. by A.R. Huffman and G.L. Bowers), *AAPG Mem.*, **76**, 177–215.

BROWN, A.R. (1996) Interpretation of three-dimensional seismic data, *AAPG Mem.*, **42**, 4th edn.

BROWN, K.M. (1990) The nature and hydrogeologic significance of mud diapirs and diatremes for accretionary systems. *J. Geophys. Res.*, **95 (B)**, 8969–8982.

CALVES, G., HUUSE, M., SCHWAB, A. & CLIFT, P. (2008) Three-dimensional seismic analysis of high-amplitude anomalies in the shallow subsurface of the Northern Indus Fan: Sedimentary and/or fluid origin. *J. Geophys. Res*., **113**, B11103.

CALVES, G. (2009) *Tectono-stratigraphic and climatic record of the NE Arabian Sea*. Ph.D. Thesis, University of Aberdeen, 292 pp.

CARTWRIGHT, J. (2007) The impact of 3D seismic data on the understanding of compaction, fluid flow and diagenesis in sedimentary basins, *J. Geol. Soc. Lond.*, **164**, 881–893.

CHAMOT-ROOKE, N., RABAUTE, A. & KREEMER, C. (2005) Western Mediterranean Ridge mud belt correlates with active shear strain at the prism-backstop geological contact. *Geology*, **33**, 861–864.

CLIFT, P.D. (2006) Controls on the erosion of Cenozoic Asia and the flux of clastic sediment to the ocean. *Earth Planet. Sci. Lett.*, **241**, 571–580.

CLIFT, P.D., GAEDICKE, C., EDWARDS, R., IL LEE, J., HILDEBRAND, P., AMJAD, S., WHITE, R.S. & SCHLATER, H.E. (2002) The stratigraphic evolution of the Indus Fan and the history of sedimentation in the Arabian Sea. *Mar. Geophys. Res.*, **23**, 223–245.

CLIFT, P.D., SHIMIZU, N., LAYNE, G.D., BLUSZTAJN, J.S., GAEDICKE, C., SCHULTER, H.-U., CLARK, M.K. & AMJAD, S. (2001) Development of the Indus Fan and its significance for the erosional history of the Western Himalaya and Karakoram. *Geol. Soc. Am. Bull.*, **113**, 1039–1051.

COLLIER, J.S. & WHITE, R.S. (1990) Mud diapirism within Indus fan sediments: Murray Ridge, Gulf of Oman. *Geophys. J. Int.*, **101**, 345–353.

CONVERSE, D.R., NICHOLSON, P.H., POTTORF, R.J. & MILLER, T.W. (2000) Controls on overpressure in rapidly subsiding basins and implications for failure of top seal. *AAPG Mem.*, **73**, 133–150.

COOPER, C. (2001) Mud volcanoes of the South Caspian Basin - Seismic data and implications for hydrocarbon systems (extended abstract). *AAPG Conv. Abs.*

DAVIES, R.J. & STEWART, S.A. (2005) Emplacement of giant mud volcanoes in the South Caspian Basin: 3D seismic reflection imaging of their root zones. *J. Geol. Soc. Lond.*, **162**, 1–4.

DAVIES, R.J., SWARBRICK, R.E., EVANS, R.J. & HUUSE, M. (2007) Birth of a mud volcano: East Java, 29 May 2006. *GSA Today*, **17**, 4–9.

DELISLE, G. (2004) The mud volcanoes of Pakistan. *Env. Geol.*, **46**, 1024–1029.

DELISLE, G., VON RAD, U., ANDRULEIT, H., VON DANIELS, C., TABREZ, A. & INAM, A. (2002) Active mud volcanoes on- And offshore eastern Makran, Pakistan. *Int. J. Earth Sci.*, **91**, 93–110.

DEPTUCK, M.E., STEFFENS, G.S., BARTON, M. & PIRMEZ, C. (2003) Architecture and evolution of upper fan channel-belts on the Niger Delta slope and in the Arabian Sea. *Mar. Pet. Geol.*, **20**, 649–676.

DEVILLE, E., BATTANI, A., GRIBOULARD, R., GUERLAIS, S., HERBIN, J.P., HOUZAY, J.P., MULLER, C. & PRINZHOFER A. (2003) The origin and processes of mud volcanism: new insights from Trinidad. In: *Subsurface sediment mobilization* (Ed. by P. van Rensbergen, R.R. Hillis, A.J. Maltman, & C.K. Morley), *Geol. Soc. Spec. Publ.*, **216**, 475–490.

DEVILLE, E., GUERLAIS, S.-H., CALLEC, Y., GRIBOULARD, R., HUYGHE, P., LALLEMANT, S., MASCLE, A., NOBLE, M., SCHMITZ, J. & the collaboration of the Caramba working group (2006) Liquefied vs stratified sediment mobilization processes: Insight from the South of the Barbados accretionary prism. *Tectonophysics*, **428**, 33–47.

DIA, A.N., CASTREC-ROUELLE, M., BOULEGUE, J. & COMEAU, P. (1999) Trinidad mud volcanoes: where do the expelled fluids come from?. *Geochim. Cosmochim. Acta*, **63**, 1023–1038.

DIMITROV, L.I. (2002) Mud volcanoes - the most important pathway for degassing deeply buried sediments. *Earth Sci. Rev.*, **59**, 49–76.

DROZ, L. & BELLAICHE, G. (1991) Seismic facies and geologic evolution of the central portion of the Indus Fan. In: *Seismic facies and sedimentary processes of submarine fans and turbidite systems* (Ed. by P. Weimer & M. H. Link), 383–402. Springer Verlag, Berlin.

ELLOUZ-ZIMMERMANN, N., DEVILLE, E., MULLER, C., LALLEMANT, S., SUBHANI, A.B. & TABREEZ, A.R. (2007) Impact of Sedimentation on Convergent Margin Tectonics: Example of the Makran Accretionary Prism, Chapter 17. In: *Thrust Belts and Foreland Basins From Fold Kinematics to Hydrocarbon Systems*, Series: Frontiers in Earth Sciences (Ed. By: O. Lacombe, J. Lavé, F. Roure, & J. Verges) , XXIV, 327-350. Springer Verlag, Berlin.

EVANS, R.J., STEWART, S.A. & DAVIES, R.J. (2008) The structure and formation of mud volcano summit calderas. *J. Geol. Soc. Lond.*, **165**, 769–780.

EVANS, R.J., DAVIES, R.J. & STEWART, S.A. (2007) Internal structure and eruptive history of a kilometre-scale mud volcano system, South Caspian Sea. *Basin Res.*, **19**, 153–163.

FOWLER, S.R., MILDENHALL, J., ZALOVA, S., RILEY, G., ELSLEY, G., DESPLANQUES, A. & GULIYEV, F. (2000) Mud volcanoes and structural development on Shah Deniz. *J. Petrol. Sci. Eng.*, **28**, 189–206.

GAEDICKE, C., SCHULTER, H., ROESER, H.A., PREXL, A., SCHRECKENBERGER, B., MEYER, H., REICHERT, C., CLIFT, P. & AMJAD, S. (2002) Origin of the northern Indus Fan and Murray Ridge, Northern Arabian Sea: interpretation from seismic and magnetic imaging. *Tectonophysics*, **355**, 127–143.

GRAUE, K. (2000) Mud volcanoes in deepwater Nigeria. *Mar. Pet. Geol.*, **17**, 959–974.

GREINERT, J., ARTEMOV, Y., EGOROV, V., De BATIST, M. & McGINNIS, D. (2006) 1300-m-high rising bubbles from mud volcanoes at 2080 m in the Black Sea: Hydroacoustic characteristics and temporal variability. *Earth Planet. Sci. Lett.*, **244**, 1–15.

GRIBOULARD, R., BOBIER, C., FAUGERES, J.C. & VERNETTE, G. (1991) Clay diapiric structures within the strike-slip margin of the southern leg of the Barbados prism. *Tectonophysics*, **192**, 383–400.

GUTIERREZ, M. & WANGEN, M. (2005) Modeling of compaction and overpressuring in sedimentary basins. *Mar. Pet. Geol.*, **22**, 351–363.

HADLER-JACOBSEN, F., GARDNER, M.H. & BORER, J.M. (2007) Seismic stratigraphic and geomorphic analysis of deep-marine deposition along the West African continental margin. In: *Seismic Geomorphology* (Ed. by R.J.

Davies, H.W., Posamentier, L.J. Wood, & J.A. Cartwright), *Geol. Soc. Spec. Publ.*, **277**, 47–84.

HEDBERG, H.D. (1980) Methane generation and petroleum migration. In: *Problems of Petroleum Migration* (Ed by: Roberts W.H. III & R.J. Cordell) *American Association of Petroleum Geologists, Studies in Geology,* **10**, 179–206.

HENRY, P., Le PICHON, X., LALLEMANT, S., LANCE, S., MARTIN, J.B., FOUCHER, J.-P., FIALA-MEDIONI, A., ROSTEK, F., GUILHAUMOU, N., PRANAL, V. & CASTREC, M. (1996) Fluid flow in and around a mud volcano field seaward of the Barbados accretionary wedge: Results from Manon cruise. *J. Geophys. Res*., **101 (B)**, 20297–20323.

HENRY, P., Le PICHON, X., LALLEMANT, S., FOUCHER, J.-P., WESTBROOK, G. & HOBART, M. (1990) Mud volcano field seaward of the Barbados accretionary complex: a deep-towed side scan sonar survey. *J. Geophys. Res*., **95 (B)**, 8917–8929.

IVANOV, M.K., LIMONOV, A.F. & VAN WEERING, T.C.E. (1996) Comparative characteristics of the Black Sea and Mediterranean Ridge mud volcanoes. *Mar. Geol.*, **132**, 253–271.

JUDD, A.G. & HOVLAND, H. (2007) *Seabed fluid flow. Impact on Geology, Biology, and the Marine Environment,* Cambridge University Press, Cambridge.

JUDD, A.G., HOVLAND, M., DIMITROV, L.I., GARCIA GIL, S. & JUKES, V. (2002) The geological methane budget at continental margins and its influence on climate change. *Geofluids*, **2**, 109–126.

KOLLA, V. & COUMES, F. (1987) Morphology, Internal Structure, Seismic Stratigraphy, and Sedimentation of Indus Fan. *AAPG Bull.*, **71**, 650–677.

KOPF, A., KLAESCHEN, D. & MASCLE, J. (2001) Extreme efficiency of mud volcanism in dewatering accretionary prisms. *Earth Planet. Sci. Lett.*, **189**, 295–313.

KOPF, A.J. (2003) Global methane emission through mud volcanoes and its past and present impact on the Earth's climate. *Int. J. Earth Sci.*, **92**, 806–816.

KOPF, A.J. (2002) Significance of mud volcanism. *Rev. Geophys.*, **40**, 1005.

KOPF, A. & BEHRMANN, J.H. (2000) Extrusion dynamics of mud volcanoes on the Mediterranean Ridge accretionary complex. In: *Salt, Shale and Igneous Diapirs in and around Europe* (Ed. by: B.C. Vendeville, Y. Mart & J.-L. Vigneresse), *Geol. Soc. Spec. Publ.*, **174**, 169–204.

LEIFER, I., LUYENDYK, B.P., BOLES, J. & CLARK, J.F. (2006) Natural marine seepage blowout: Contribution to atmospheric methane. *Global Biogeochem. Cycles*, **20**, 1–9.

LØSETH, H., WENSAAS, ARNTSEN, B., HANKEN, N., BASIRE, C. & GRAUE, K. (2001) 1000 m long gas blow-out pipes. *Extended Abstract Volume 63rd EAGE Conference & Exhibition*.

MALTMAN, A.J. & BOLTON, A. (2003) How sediments become mobilized. In: *Subsurface sediment mobilization*, (Ed. by: P. van Rensbergen, R.R. Hillis, A.J. Maltman & C.K. Morley), *Geol. Soc. Spec. Publ.*, **216**, 9–20.

McHARGUE, T.R., & WEBB, J.E. (1986) Internal geometry, seismic facies, and petroleum potential of canyons and inner fan channels of the Indus Submarine Fan. *AAPG Bull.*, **70**, 161–180.

METIVIER, F., GAUDEMER, Y., TAPPONNIER, P. & KLEIN, M. (1999) Mass accumulation rates in Asia during the Cenozoic. *Geophys. J. Int.*, **137**, 280–318.

MILKOV, A.V., SASSEN, R., APANASOVICH, T.V. & DADASHEV, F.G. (2003) Global gas flux from mud volcanoes: A significant source of fossil methane in the atmosphere and the ocean. *Geophys. Res. Lett.*, **30**, 1–9.

MILKOV, A.V. (2000) Worldwide distribution of submarine mud volcanoes and associated gas hydrates. *Mar. Geol.*, **167**, 29–42.

NAUDTS, L., GREINERT, J., ARTEMOV, Y., STAELENS, P., POORT, J., van RENSBERGEN, P. & De BATIST, M. (2006) Geological and morphological setting of 2778 methane seeps in the Dnepr paleo-delta, northwestern Black Sea. *Mar. Geol.*, **227**, 177–199.

NEWTON, R.S., CUNNINGHAM, R.C. & SCHUBERT, C.E. (1980) Mud volcanoes and pockmarks: Seafloor engineering hazards or geological curiosities? *Offshore Tech. Conf.,* **12**, 425–435.

OSBORNE, M.J. & SWARBRICK, R.E. (1997) Mechanisms for generating overpressure in sedimentary basins: A reevaluation. *AAPG Bull.*, **81**, 1023–1041.

REVIL, A. (2002) Genesis of mud volcanoes in sedimentary basins: A solitary wave-based mechanism. *Geophys. Res. Lett.*, **29**, 15–1.

ROBERTSON, A.H.F. & KOPF, A. (1998) Tectonic setting and processes of mud volcanism on the Mediterranean Ridge accretionary complex: evidence from Leg 160. In: *Proc. ODP, Sci. Results,* **160** (Ed. by: A.H.F. Robertson, K.-C. Emeis, C. Richter & A. Camerlenghi) College Station, TX (Ocean Drilling Program), 665–680.

SAUTER, E.J., MUYAKSHIN, S.I., CHARLOU, J., SCHULTER, M., BOETIUS, A., JEROSCH, K., DAMM, E., FOUCHER, J. & KLAGES, M. (2006) Methane discharge from a deep-sea submarine mud volcano into the upper water column by gas hydrate-coated methane bubbles. *Earth Planet. Sci. Lett.*, **243**, 354–365.

SCLATER, J.G. & CHRISTIE, P.A.F. (1980) Continental stretching: An explanation of the post-mid-Cretaceous subsidence of the Central North Sea basin. *J. Geophys. Res*., **85 (B)**, 3711–3739.

SOMOZA, L., GARDNER, J. M., DIAZ-DEL-RIO, V., VAZQUEZ, J. T., PINHEIRO, L.M. & HERNANDEZ-MOLINA, F.J. (2002) Numerous methane gas-related sea floor structures identified in Gulf of Cadiz, *Eos Trans. AGU*, **83(47)**, 541.

STEWART, S.A. & DAVIES, R.J. (2006) Structure and emplacement of mud volcano systems in the South Caspian Basin. *AAPG Bull.*, **90**, 771–786.

STIFFE, A.W. (1874) On the Mud-craters and Geological Structure of the Mekran Coast. *Q. J. Geol. Soc. Lond.*, **30**, 50–53.

SYKES, L.R. & LANDISMAN, M. (1964) Seismicity of East Africa, the Gulf of Aden and Arabian and Red Sea. *Bull. Seismol. Soc. Am.*, **54**, 1927–1940.

VAIL, P.R., MITCHUM, R.M. & THOMPSON, S. (1977) Seismic stratigraphy and global changes of sea-level, part 3: Relative changes of sea level from coastal onlap. In: *Seismic Stratigraphy-Applications to hydrocarbon exploration*, (Ed. by C.E. Payton) *AAPG Mem.*, **26**, 63–81.

van RENSBERGEN, P., DEPREITER, D., PANNEMANS, B. & HENRIET, J.-P. (2005) Seafloor expression of sediment extrusion and intrusion at the El Arraiche mud volcano field, Gulf of Cadiz. *J. Geophys. Res*., **110 (F)**, 1–13.

van RENSBERGEN, P., MORLEY, C.K., ANG, D.W., HOAN, T.Q. & LAM, N.T. (1999) Structural evolution of shale diapirs from reactive rise to mud volcanism: 3D seismic data from the Baram delta, offshore Brunei Darussalam. *J. Geol. Soc. Lond.*, **156**, 633–650.

VELDE, B. (1996) Compaction trends of clay-rich deep sea sediments. *Mar. Geol.*, **133**, 193–201.

von RAD, U., SCHULZ, H., RIECH, V., DEN DULK, M., BERNER, U. & SIROCKO, F. (1999) Multiple monsoon-controlled breakdown of oxygen-minimum conditions during the past 30,000 years documented in laminated sediments off Pakistan. *Palaeogeography, Palaeoclimatology, Palaeoecology*, **152**, 129–161.

WHITE, R.S. (1983) The Little Murray Ridge. In: *Seismic Expression of Structural Styles* (Ed. by A.W. Bally) *American Association of Petroleum Geologists, Studies in Geology,* **15**, Chapter 15, 19–23.

WHITE, R.S. & LOUDEN, K.E. (1982) The Makran continental margin: Structure of a thickly sedimented convergent plate boundary. In: S*tudies in Continental Margin Geology* (Ed. by J.S. Watkins & C.L. Drake), *AAPG Mem.*, **34**, 499–518.

YEILDING, C.A. & TRAVIS, C.J. (1997) Nature and significance of irregular geometries at the salt-sediment interface: Examples from the deepwater Gulf of Mexico (abs): *AAPG Annual Meeting Program*, **6**, A128.

YUSIFOV, M. & RABINOWITZ, P.D. (2004) Classification of mud volcanoes in the South Caspian Basin, offshore Azerbaijan. *Mar. Pet. Geol.*, **21**, 965–975.

Mud volcano	Water depth	Stratigraphic interval	Mud cone					Conduit			Overburden				Life span
	(km)		Diameter (km) Dmc	Surface (sq. km)	Thickness (km) Hmc	Volume (km3)	Total volume (km3)	Diameter (km) Dc	Height (km) Hc	Volume (km3)	Basement depth (km) Bd	Paleocene depth (km) Pd	Parent bed thickness (km) Pbt	Overburden at mud volcano base (km) Omb	m.y.
Delilah	0,668	Base Middle Miocene	5,070	20,2	0,585	3,89	3,89	2,110	3,931	4,53	7,75	6,53	1,22	2,57	1,87
Ingrid	0,781	Base Lower Miocene	8,437	55,9	0,640	11,81		1,800	3,419	2,87	8,39	7,09	1,30	1,60	5,56
		Top Lower Miocene	7,420	43,2	0,447	6,38					8,39	7,09	1,30	2,25	3,88
		Base Middle Miocene	4,563	16,3	0,390	2,10					8,39	7,09	1,30	3,00	1,25
		Upper Miocene - Pliocene	2,038	3,3	0,176	0,19	20,48				8,39	7,09	1,30	3,65	0,86
Louise	0,930	Upper Miocene	4,490	15,8	0,350	1,83		0,300	6,793	0,16	8,56	7,67	0,89	6,21	0,65
		Plio-Pleistocene	1,854	2,7	0,084	0,08	1,90				8,56	7,67	0,89	7,37	0,63
Joyce	1,080	Base Lower Miocene	4,142	13,5	0,469	5,50		1,770	4,782	3,88	8,92	7,90	1,02	1,94	4,08
		Top Lower Miocene	6,712	35,4	0,471	5,50					8,92	7,90	1,02	2,52	4,10
		Top Lower - Base Middle Miocene	6,728	35,5	0,262	3,07					8,92	7,90	1,02	2,76	0,84
		Base Middle Miocene	3,060	7,4	0,273	0,66	14,73				8,92	7,90	1,02	2,85	0,87
Catherine	1,219	Base Middle Miocene	3,092	7,5	0,247	0,61		1,876	3,405	3,10	7,07	6,15	0,92	1,46	0,79
		Middle Miocene	6,625	34,5	0,259	2,94	3,55				7,07	6,15	0,92	3,21	0,83
		Plio-Pleistocene	1,800	2,5	0,099	0,08	3,63				7,07	6,15	0,92	4,54	1,85
Anne	1,263	Upper Miocene - Pliocene - Pleistocene	0,800	0,5	0,176	0,03	0,03	0,170	0,764	0,01	6,10	5,14	0,96	3,22	0,86
Bertrand	1,315	Middle Miocene	3,772	11,2	0,296	1,09		0,815	5,717	0,98	8,13	7,08	1,05	3,51	0,95
		Upper Miocene	2,260	4,0	0,293	0,39					8,13	7,08	1,05	3,76	0,94
		Upper Miocene - Pliocene	2,254	4,0	0,273	0,36	1,84				8,13	7,08	1,05	5,23	1,34
Georgina	0,936	Top Lower Miocene	6,860	36,9	0,398	4,85		1,043	5,988	1,69	8,70	7,65	1,05	3,65	3,46
		Top Lower Miocene	7,840	48,3	0,456	7,26	12,11				8,70	7,65	1,05	3,97	3,96
Henny	0,446	Top Lower Miocene	6,845	36,78	0,765	11,13	11,130	0,72	3,118	0,419	7,9	7,65	1,12	2,31	2,45

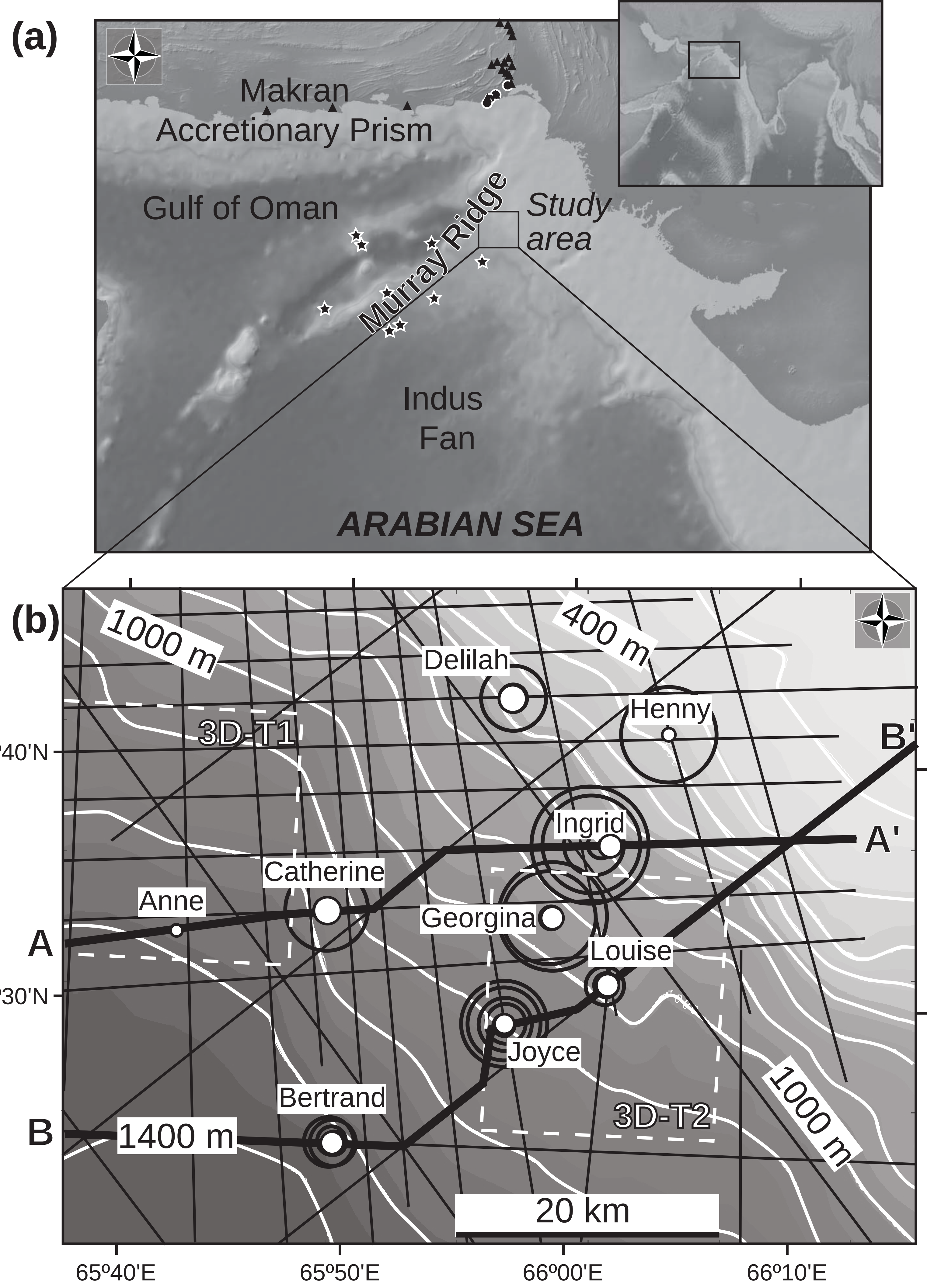

(a)
Makran
Accretionary Prism
Gulf of Oman
Murray Ridge
Study area
Indus Fan
ARABIAN SEA
(b)
1000 m
400 m
Delilah
Henny
3D-T1
23º40'N
B'
Ingrid
A'
Catherine
Anne
Georgina
A
Louise
23º30'N
Joyce
1000 m
Bertrand
B
1400 m
3D-T2
20 km
65º40'E
65º50'E
66º00'E
66º10'E

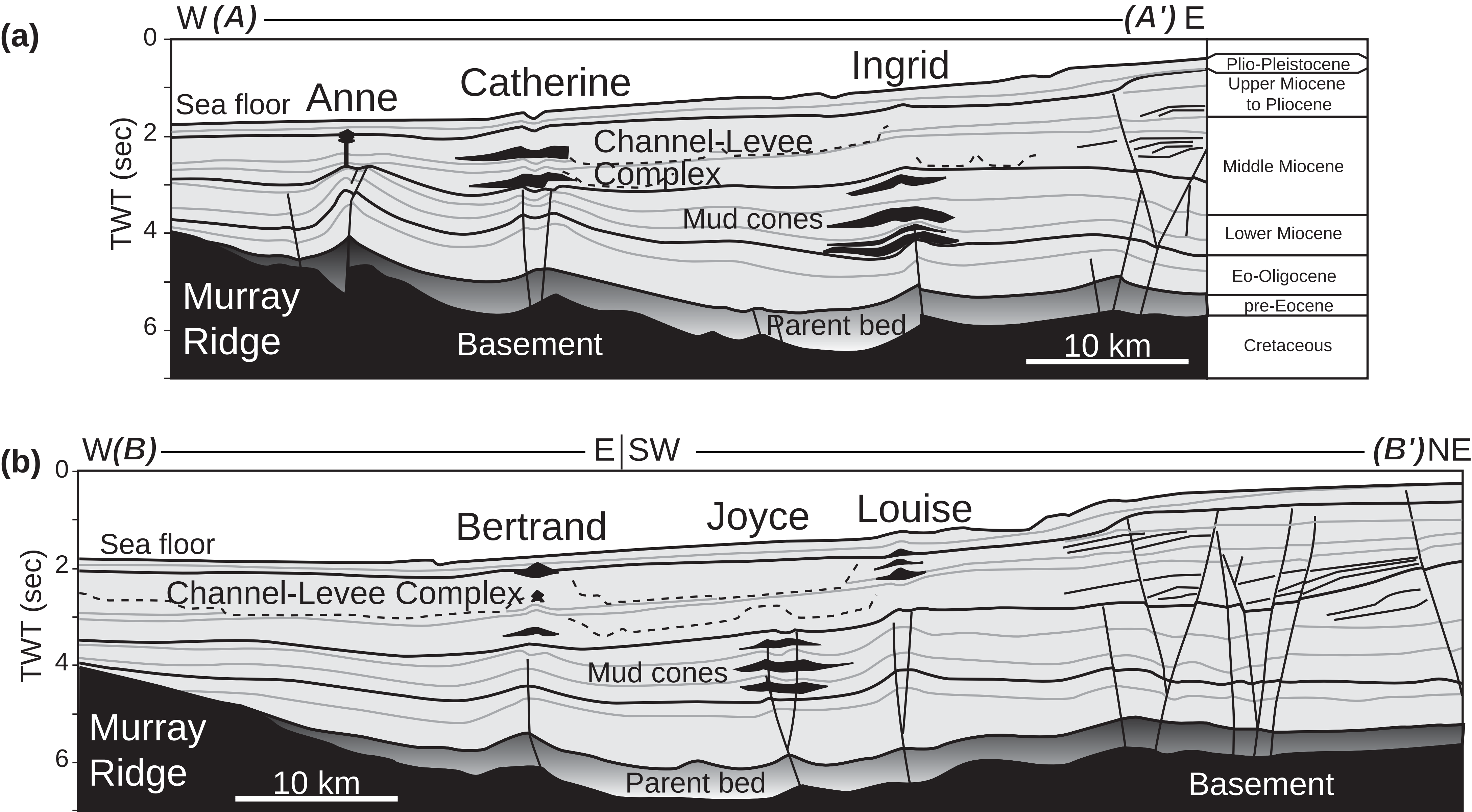

(a)
W (A)
(A') E
0
2
4
6
TWT (sec)
Sea floor
Anne
Catherine
Ingrid
Channel-Levee
Complex
Mud cones
Murray
Ridge
Basement
Parent bed
10 km
Plio-Pleistocene
Upper Miocene
to Pliocene
Middle Miocene
Lower Miocene
Eo-Oligocene
pre-Eocene
Cretaceous
(b)
W (B)
E | SW
(B') NE
0
2
4
6
TWT (sec)
Sea floor
Bertrand
Joyce
Louise
Channel-Levee Complex
Mud cones
Murray
Ridge
10 km
Parent bed
Basement

(a) Basement depth structure (km)
Strike-slip faults
Growth faults
Murray Ridge
Figure 2 a
Figure 2 b
Trough
5.5
6.5
7.5
8.5
9.5
20 km
(b) Top pre-Eocene depth structure (km)
Mud volcano field
Anticlines
5
6
7
8
(c) Isopach pre-Eocene sequence (km)
0.5
1
1.5
(d) Post - pre-Eocene isopach (km)
4
5
6
7
23º40'N
23º30'N
65º40'E
65º50'E
66º00'E
66º10'E

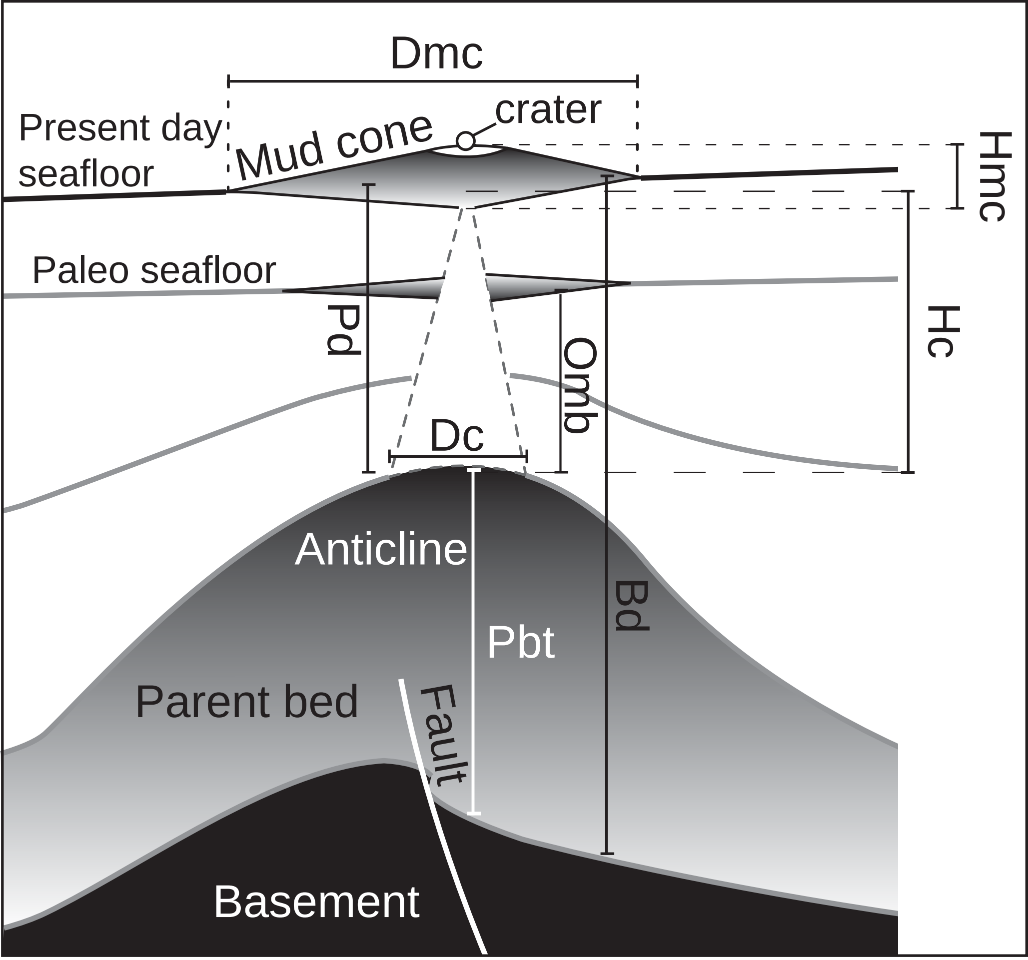

Dmc
crater
Present day seafloor
Mud cone
Hmc
Paleo seafloor
Pd
Omb
Hc
Dc
Anticline
Bd
Pbt
Parent bed
Fault
Basement

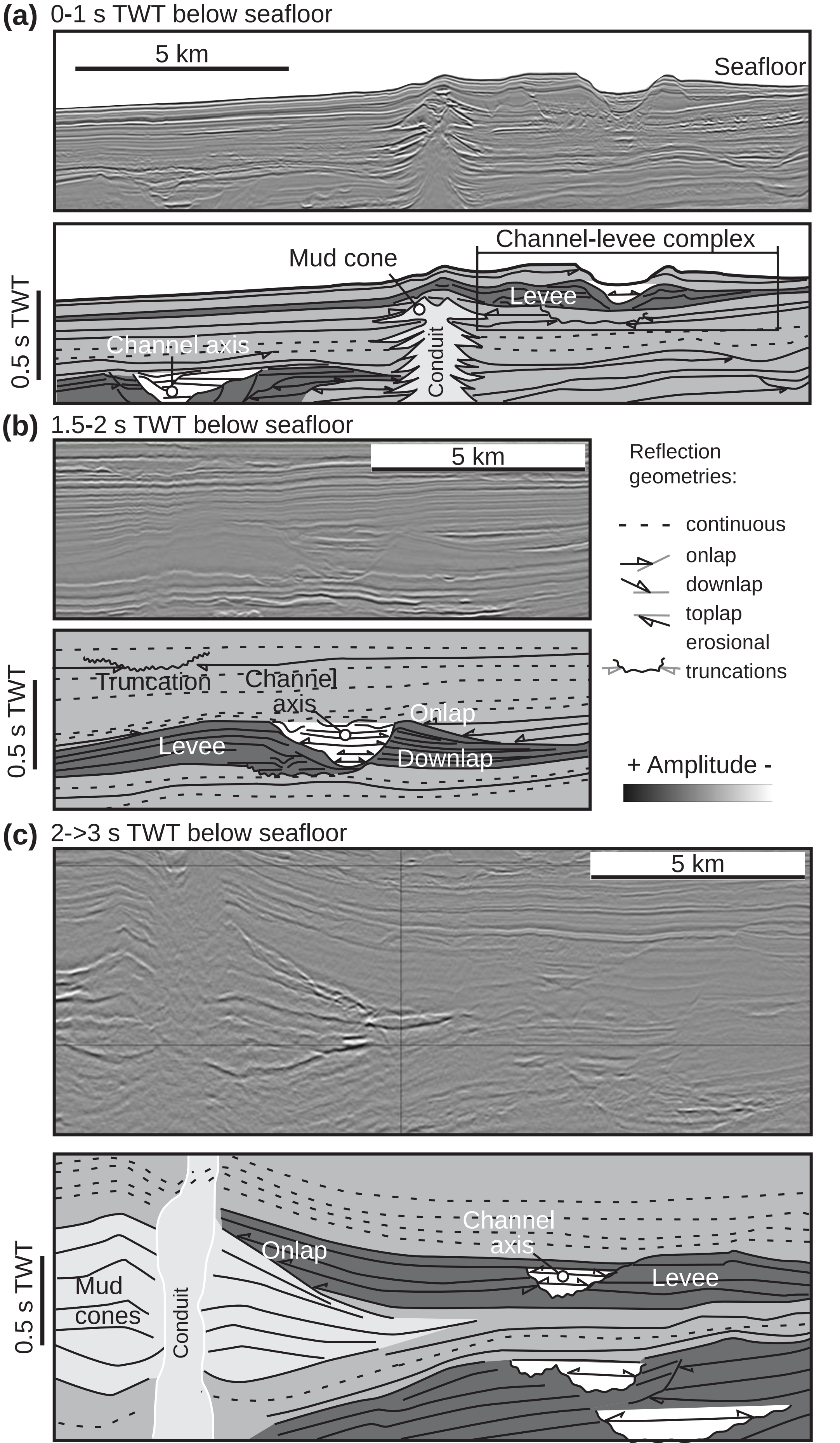
(a)
0-1 s TWT below seafloor
5 km
Seafloor
Channel-levee complex
Mud cone
Levee
0.5 s TWT
Channel axis
Conduit
(b)
1.5-2 s TWT below seafloor
5 km
Reflection geometries:
continuous
onlap
downlap
toplap
erosional truncations
Truncation
Channel axis
Onlap
Levee
Downlap
0.5 s TWT
+ Amplitude -
(c)
2->3 s TWT below seafloor
5 km
Channel axis
Onlap
Levee
Mud cones
Conduit
0.5 s TWT

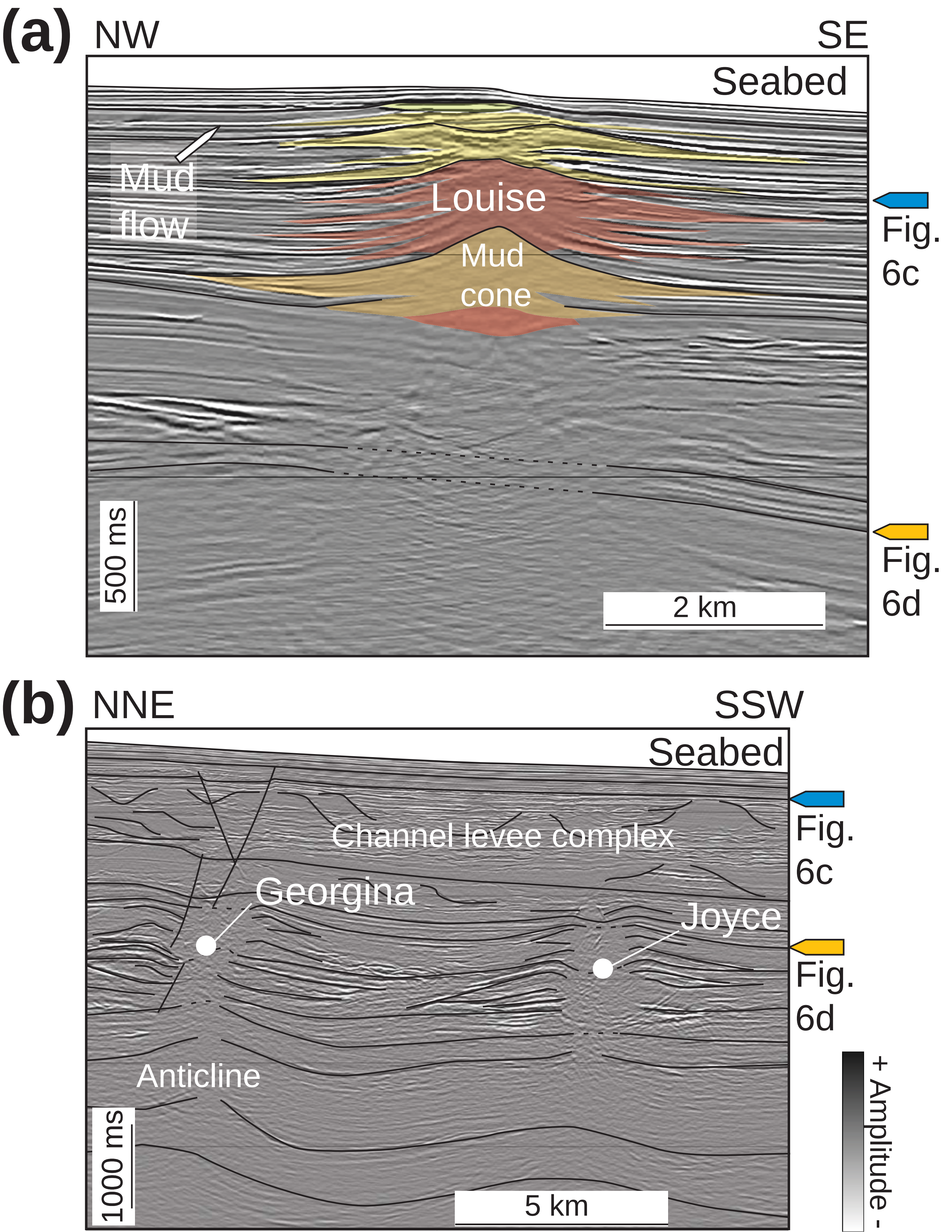
(a)
NW
SE
Seabed
Mud flow
Louise
Mud cone
Fig. 6c
Fig. 6d
500 ms
2 km
(b)
NNE
SSW
Seabed
Channel levee complex
Georgina
Joyce
Anticline
Fig. 6c
Fig. 6d
1000 ms
5 km
+ Amplitude -

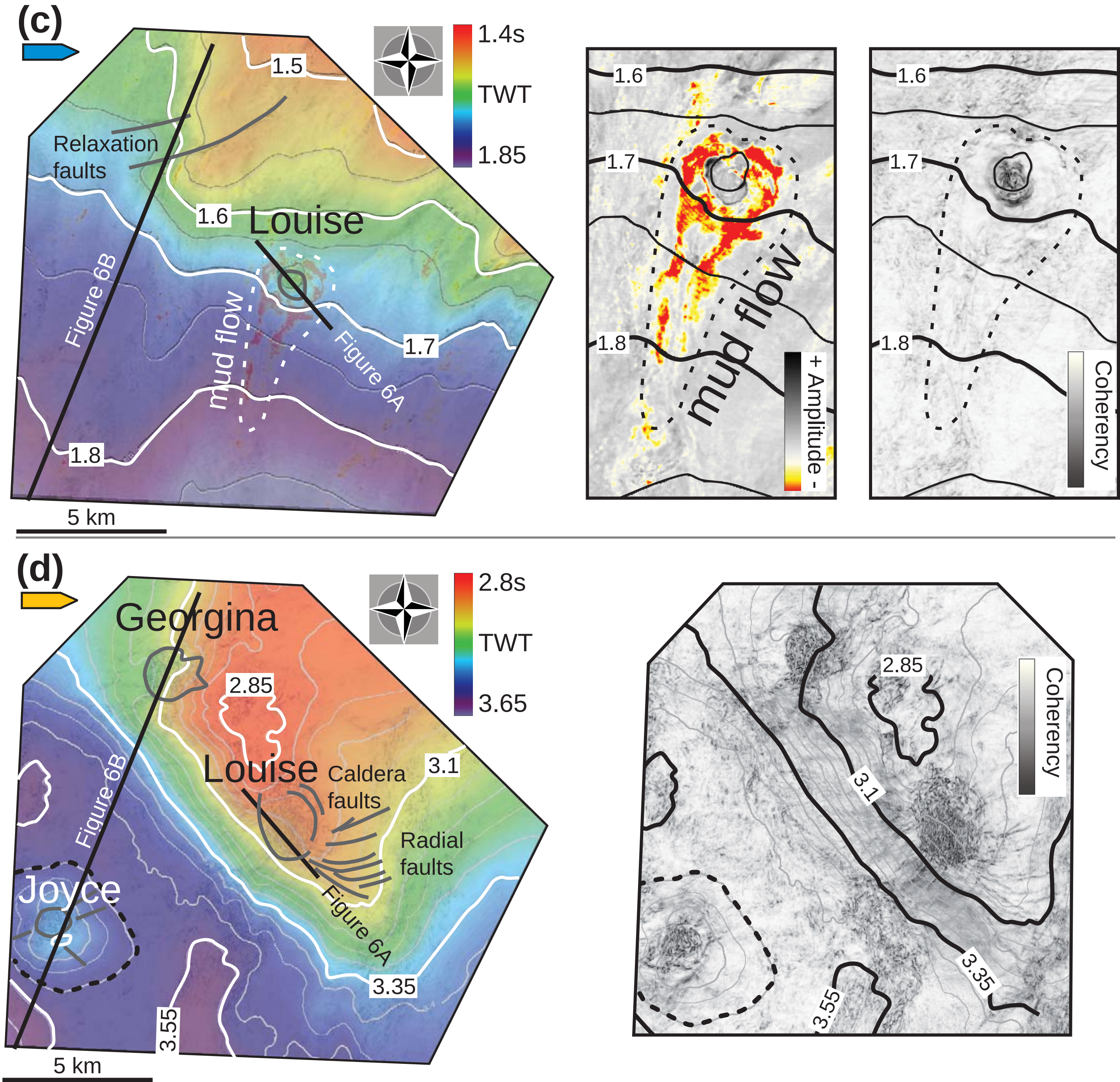

(c)
1.4s
TWT
1.85
1.5
Relaxation
faults
1.6
Louise
Figure 6B
mud flow
Figure 6A
1.7
1.8
5 km
1.6
1.7
1.8
mud flow
+ Amplitude -
Coherency
(d)
2.8s
TWT
3.65
Georgina
2.85
Louise
Caldera
faults
3.1
Radial
faults
Figure 6B
Joyce
Figure 6A
3.35
3.55
5 km
2.85
3.1
3.35
3.55
Coherency

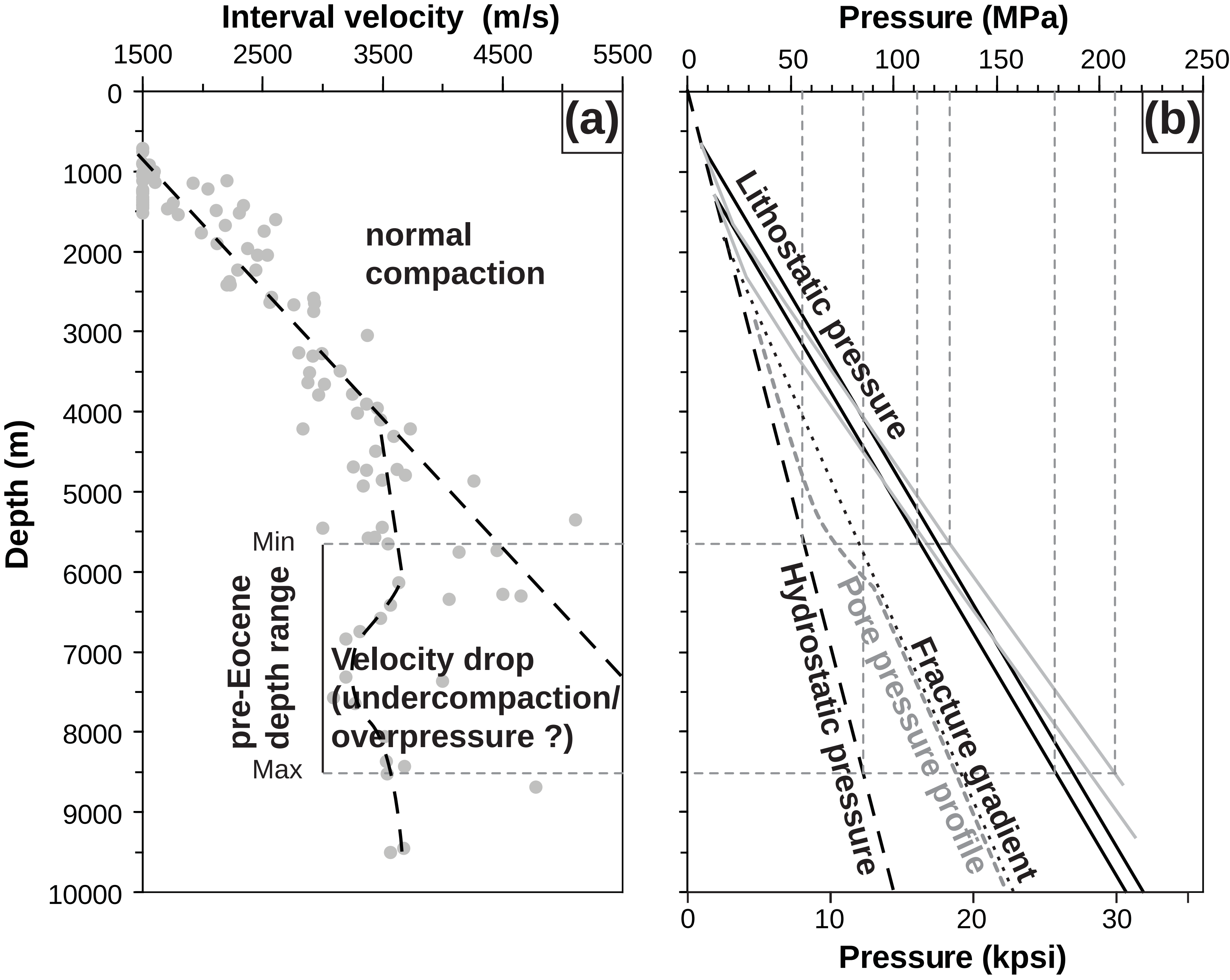

Interval velocity (m/s)
1500
2500
3500
4500
5500
Depth (m)
0
1000
2000
3000
4000
5000
6000
7000
8000
9000
10000
(a)
normal compaction
Min
Max
pre-Eocene depth range
Velocity drop (undercompaction/ overpressure ?)
Pressure (MPa)
0
50
100
150
200
250
(b)
Lithostatic pressure
Hydrostatic pressure
Pore pressure profile
Fracture gradient
0
10
20
30
Pressure (kpsi)

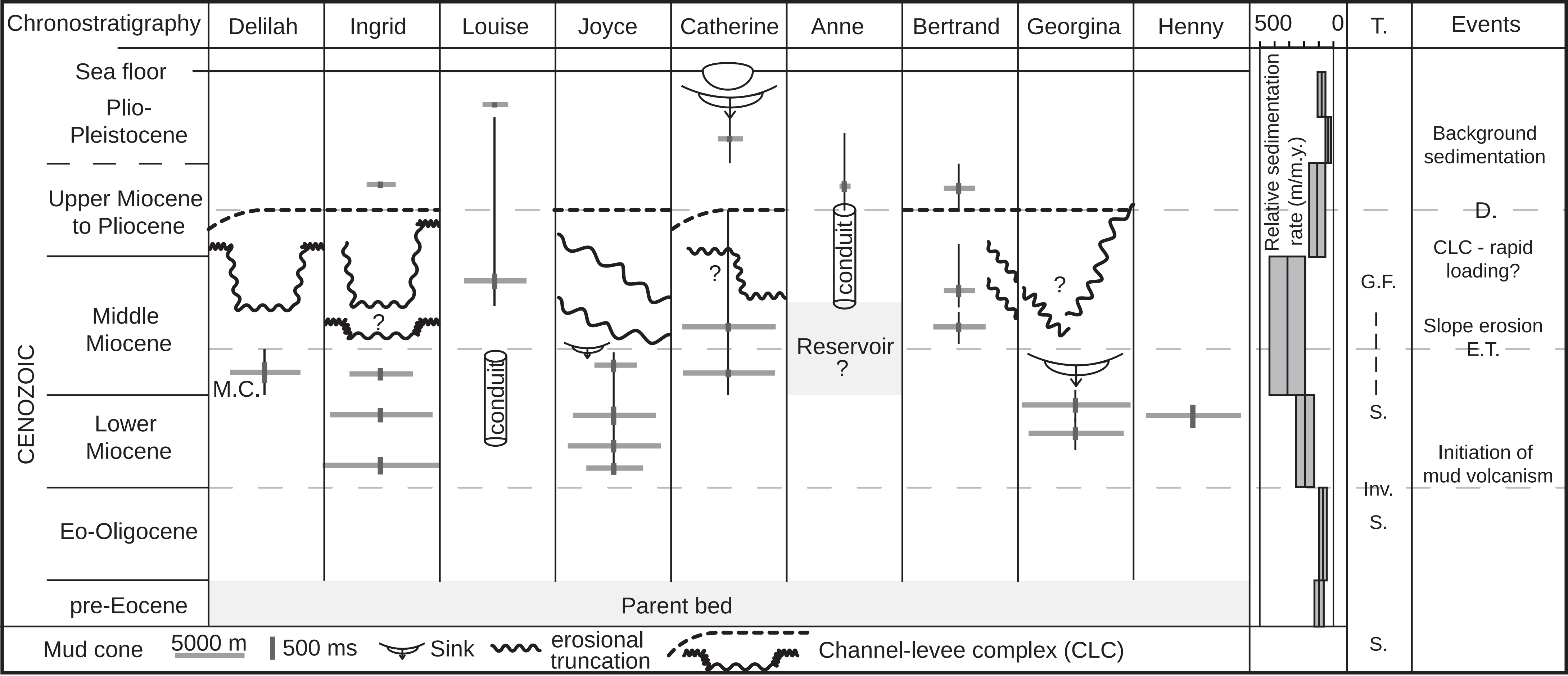
Chronostratigraphy
Delilah
Ingrid
Louise
Joyce
Catherine
Anne
Bertrand
Georgina
Henny
500
0
T.
Events
Sea floor
Plio-Pleistocene
Upper Miocene to Pliocene
Middle Miocene
Lower Miocene
Eo-Oligocene
pre-Eocene
CENOZOIC
M.C.
conduit
conduit
Reservoir ?
Parent bed
Relative sedimentation rate (m/m.y.)
G.F.
S.
Inv.
S.
S.
Background sedimentation
D.
CLC - rapid loading?
Slope erosion
E.T.
Initiation of mud volcanism
Mud cone
5000 m
500 ms
Sink
erosional truncation
Channel-levee complex (CLC)

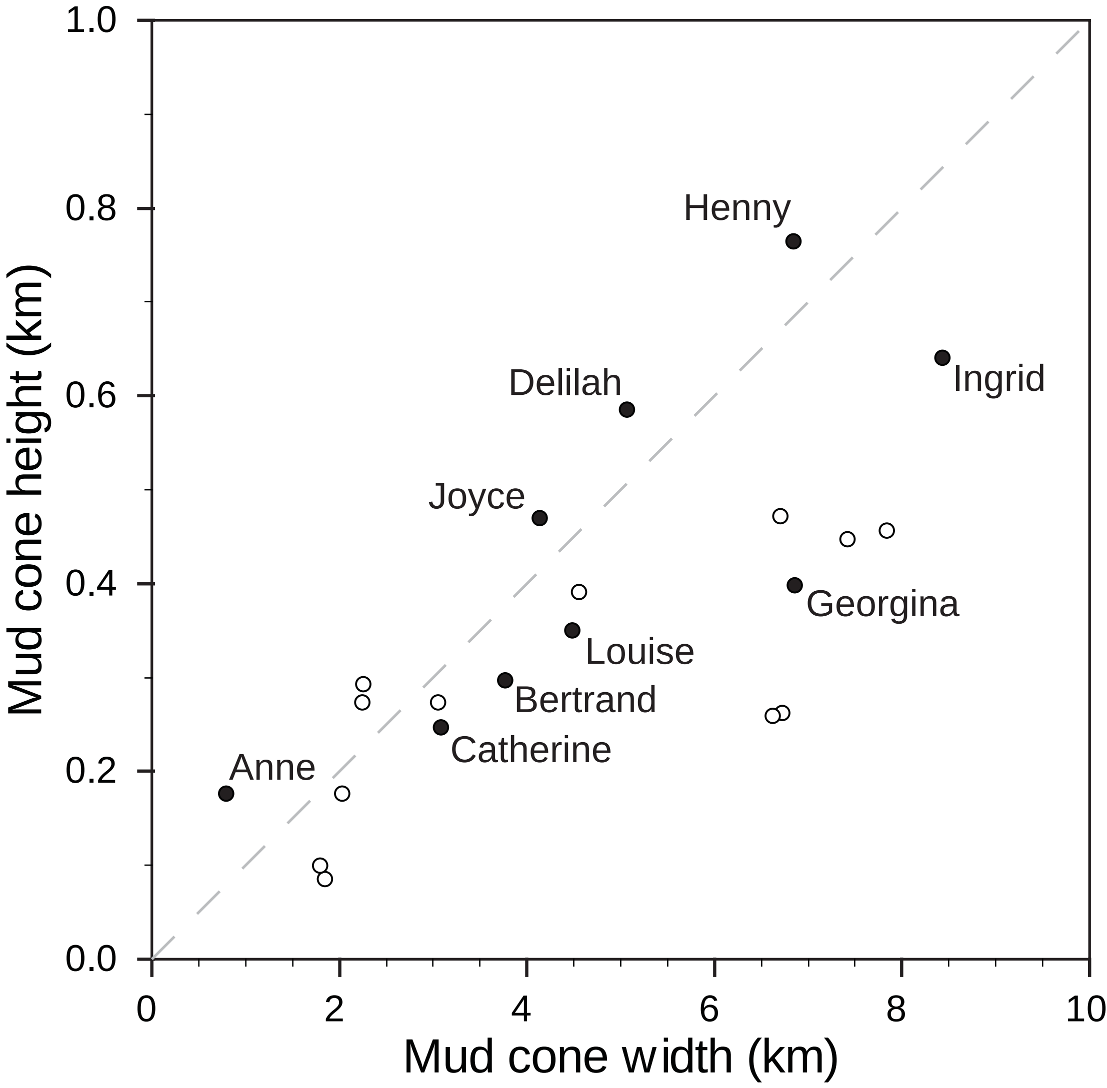
1.0
0.8
0.6
0.4
0.2
0.0
0
2
4
6
8
10
Mud cone height (km)
Mud cone width (km)
Henny
Ingrid
Delilah
Joyce
Georgina
Louise
Bertrand
Catherine
Anne

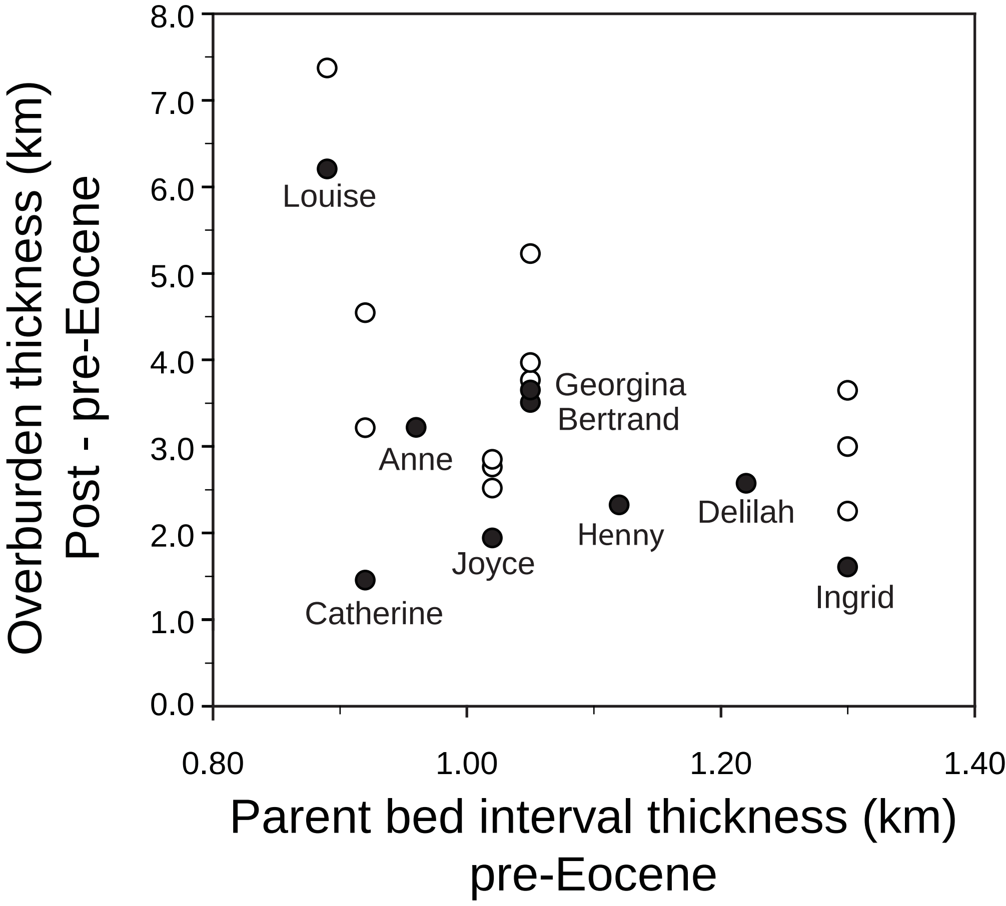
Overburden thickness (km)
Post - pre-Eocene
8.0
7.0
6.0
5.0
4.0
3.0
2.0
1.0
0.0
Louise
Georgina
Bertrand
Anne
Delilah
Henny
Joyce
Ingrid
Catherine
0.80
1.00
1.20
1.40
Parent bed interval thickness (km)
pre-Eocene

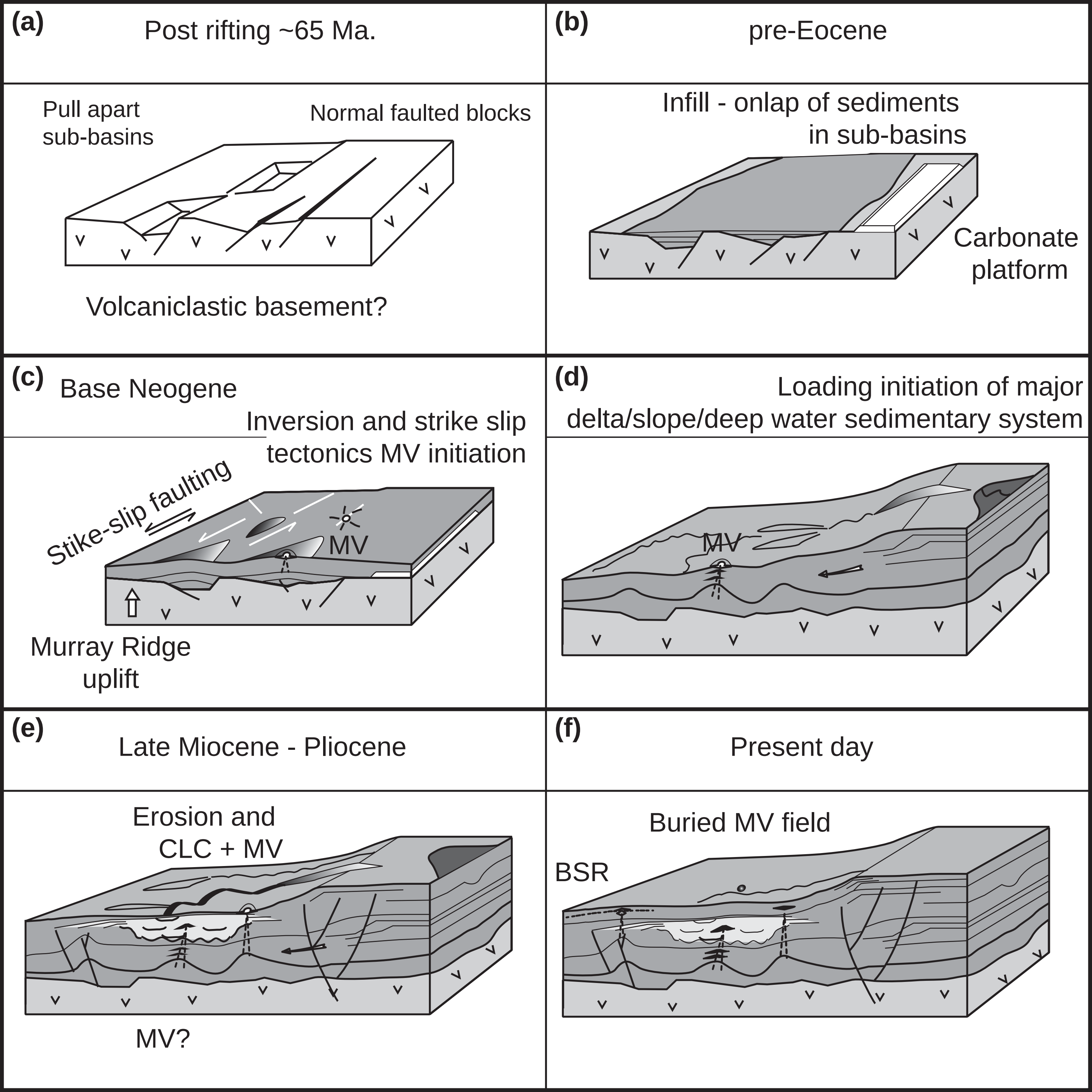

(a)
Post rifting ~65 Ma.
Pull apart
sub-basins
Normal faulted blocks
Volcaniclastic basement?
(b)
pre-Eocene
Infill - onlap of sediments
in sub-basins
Carbonate
platform
(c)
Base Neogene
Inversion and strike slip
tectonics MV initiation
Stike-slip faulting
MV
Murray Ridge
uplift
(d)
Loading initiation of major
delta/slope/deep water sedimentary system
MV
(e)
Late Miocene - Pliocene
Erosion and
CLC + MV
MV?
(f)
Present day
Buried MV field
BSR

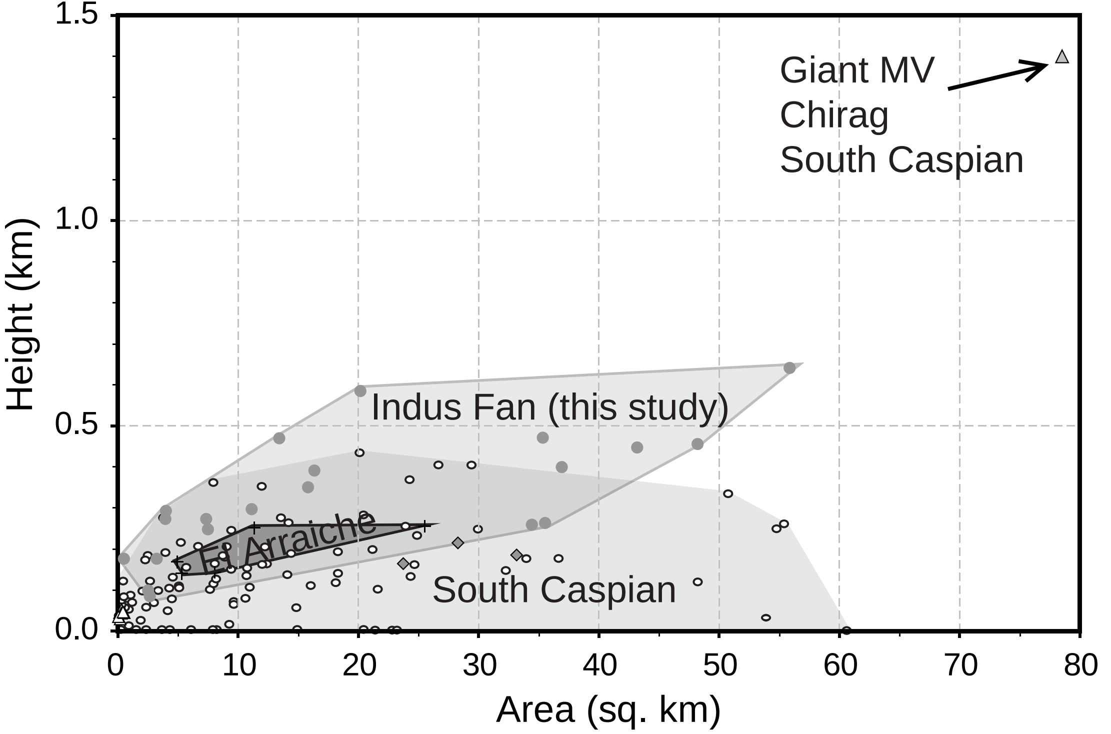

1.5
1.0
0.5
0.0
Height (km)
0
10
20
30
40
50
60
70
80
Area (sq. km)
Giant MV
Chirag
South Caspian
Indus Fan (this study)
El Arraiche
South Caspian